Journal Pre-proof

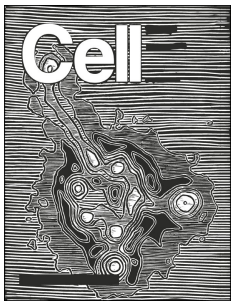

Reduced neutralization of SARS-CoV-2 B.1.617 by vaccine and convalescent serum

Chang Liu, Helen M. Ginn, Wanwisa Dejnirattisai, Piyada Supasa, Beibei Wang, Aekkachai Tuekprakhon, Rungtiwa Nutalai, Daming Zhou, Alexander J. Mentzer, Yuguang Zhao, Helen M.E. Duyvesteyn, César López-Camacho, Jose Slon-Campos, Thomas S. Walter, Donal Skelly, Sile Ann Johnson, Thomas G. Ritter, Chris Mason, Sue Ann Costa Clemens, Felipe Gomes Naveca, Valdinete Nascimento, Fernanda Nascimento, Cristiano Fernandes da Costa, Paola Cristina Resende, Alex Pauvolid-Correa, Marilda M. Siqueira, Christina Dold, Nigel Temperton, Tao Dong, Andrew J. Pollard, Julian C. Knight, Derrick Crook, Teresa Lambe, Elizabeth Clutterbuck, Sagida Bibi, Amy Flaxman, Mustapha Bittaye, Sandra Belij-Rammerstorfer, Sarah C. Gilbert, Tariq Malik, Miles W. Carroll, Paul Klenerman, Eleanor Barnes, Susanna J. Dunachie, Vicky Baillie, Natali Serafin, Zanele Ditse, Kelly Da Silva, Neil G. Paterson, Mark A. Williams, David R. Hall, Shabir Madhi, Marta C. Nunes, Philip Goulder, Elizabeth E. Fry, Juthathip Mongkolsapaya, Jingshan Ren, David I. Stuart, Gavin R. Screaton

PII: S0092-8674(21)00755-8

DOI: https://doi.org/10.1016/j.cell.2021.06.020

Reference: CELL 12094

To appear in: *Cell*

Received Date: 25 May 2021

Revised Date: 4 June 2021

Accepted Date: 11 June 2021

Please cite this article as: Liu, C., Ginn, H.M., Dejnirattisai, W., Supasa, P., Wang, B., Tuekprakhon, A., Nutalai, R., Zhou, D., Mentzer, A.J., Zhao, Y., Duyvesteyn, H.M.E., López-Camacho, C., Slon-Campos, J., Walter, T.S., Skelly, D., Johnson, S.A., Ritter, T.G., Mason, C., Costa Clemens, S.A., Naveca, F.G., Nascimento, V., Nascimento, F., Fernandes da Costa, C., Resende, P.C., Pauvolid-Correa, A., Siqueira, M.M., Dold, C., Temperton, N., Dong, T., Pollard, A.J., Knight, J.C., Crook, D., Lambe, T., Clutterbuck, E., Bibi, S., Flaxman, A., Bittaye, M., Belij-Rammerstorfer, S., Gilbert, S.C., Malik, T., Carroll, M.W., Klenerman, P., Barnes, E., Dunachie, S.J., Baillie, V., Serafin, N., Ditse, Z., Da Silva, K., Paterson, N.G., Williams, M.A., Hall, D.R., Madhi, S., Nunes, M.C, Goulder, P., Fry, E.E., Mongkolsapaya, J., Ren, J., Stuart, D.I., Screaton, G.R., Reduced neutralization of SARS-CoV-2 B.1.617 by vaccine and convalescent serum, *Cell* (2021), doi: https://doi.org/10.1016/j.cell.2021.06.020.

Reduced neutralization but no widespread escape of B.1.617.2

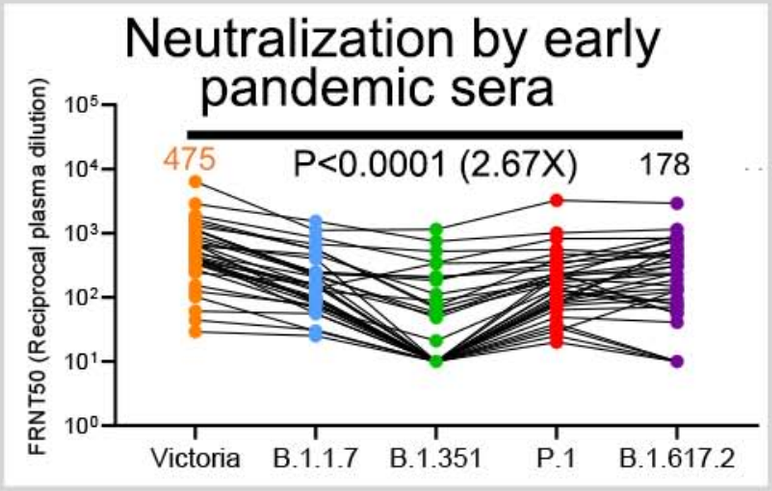

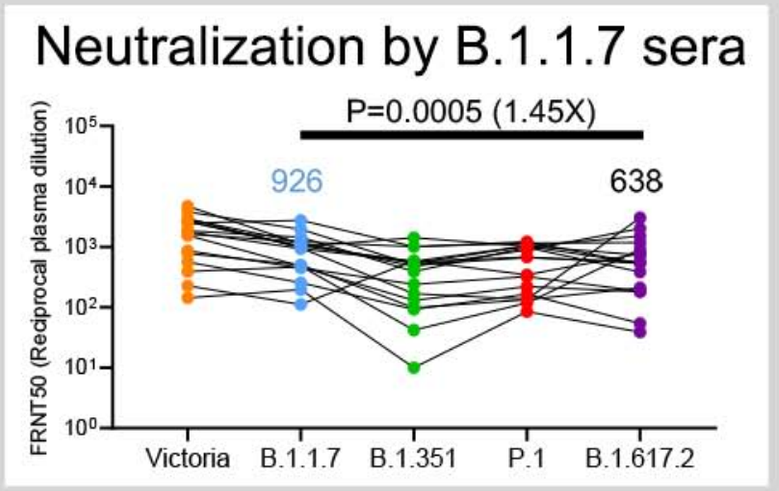

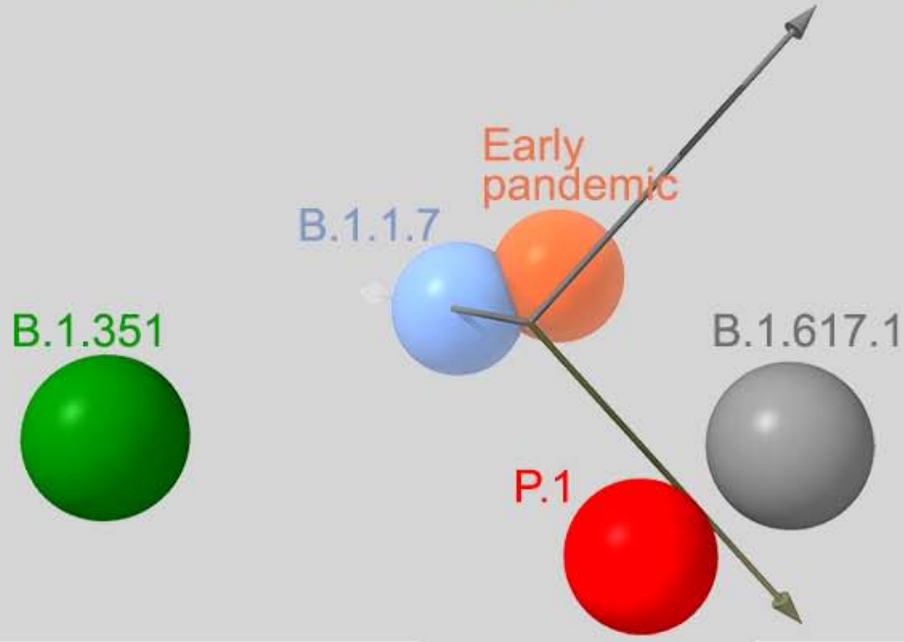

SARS-CoV-2 antigenic space plot suggests early pandemic and B1.1.7 based vaccines likely to give broadest protection against current variants

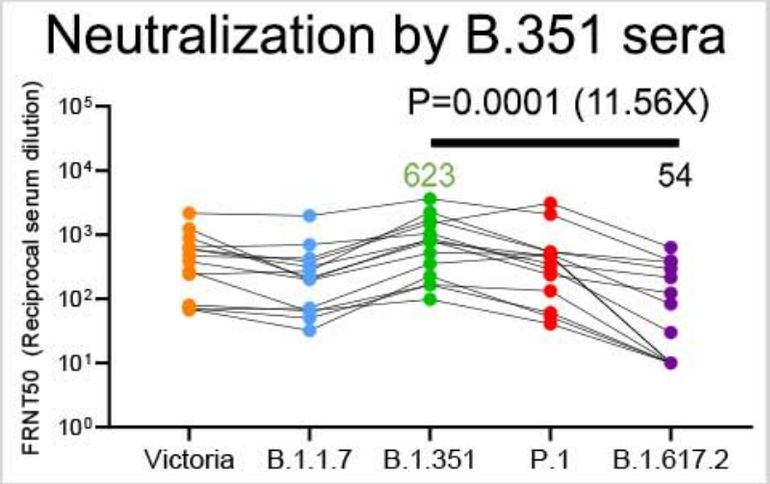

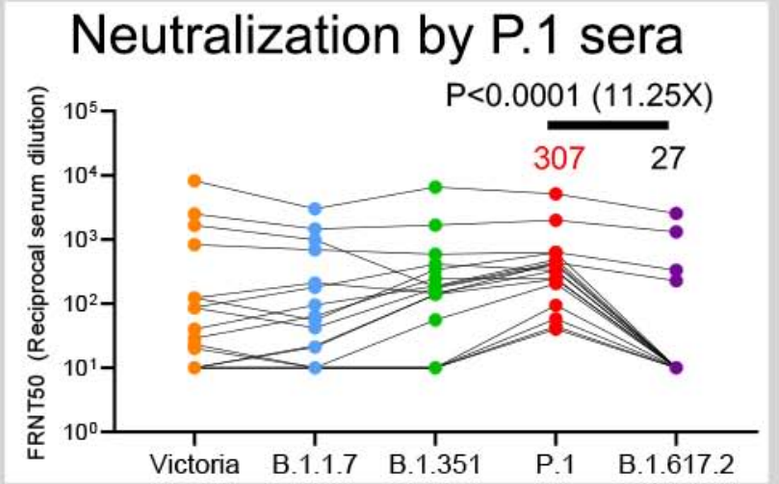

Reduced neutralization of SARS-CoV-2 B.1.617 by vaccine and convalescent serum

Chang Liu[#,1,2], Helen M. Ginn[#,3], Wanwisa Dejnirattisai[#1], Piyada Supasa[#,1], Beibei Wang[#1], Aekkachai Tuekprakhon[#.1], Rungtiwa Nutalai[#1], Daming Zhou[#,4],Alexander J. Mentzer[#,1,5], Yuguang Zhao[4], Helen M.E. Duyvesteyn[4], César López-Camacho[1], Jose Slon-Campos[1], Thomas S. Walter[4], Donal Skelly[5,6,7], Sile Ann Johnson[6], Thomas G. Ritter[5], Chris Mason[5], Sue Ann Costa Clemens[8], Felipe Gomes Naveca[9], Valdinete Nascimento[9], Fernanda Nascimento[9], Cristiano Fernandes da Costa[10], Paola Cristina Resende[11], Alex Pauvolid-Correa[11,12], Marilda M. Siqueira[11], Christina Dold[13,14], Nigel Temperton[15],Tao Dong[2,16,17], Andrew J. Pollard[13,14], Julian C. Knight[1,2,16], Derrick Crook[16], Teresa Lambe[18], Elizabeth Clutterbuck[13,14], Sagida Bibi[13,14], Amy Flaxman[18], Mustapha Bittaye[18], Sandra Belij-Rammerstorfer[18], Sarah C. Gilbert[18], Tariq Malik[19], Miles W. Carroll[1,19], Paul Klenerman[5,6,13,20], Eleanor Barnes[5,6,13,20], Susanna J. Dunachie,[5,6,21,22], Vicky Baillie[23,24], Natali Serafin[23,24], Zanele Ditse[23,24], Kelly Da Silva[23,24], Neil G. Paterson[3], Mark A. Williams[3], David R. Hall[3], Shabir Madhi[23,24], Marta C Nunes[23,24], Philip Goulder[6], Elizabeth E. Fry[4], Juthathip Mongkolsapaya[1,2,25,*,] Jingshan Ren[4,*], David I. Stuart[1,2,3,4,26*§], and Gavin R. Screaton[1,2,*]

1. Wellcome Centre for Human Genetics, Nuffield Department of Medicine, University of Oxford, Oxford, UK
2. Chinese Academy of Medical Science (CAMS) Oxford Institute (COI), University of Oxford, Oxford, UK
3. Diamond Light Source Ltd, Harwell Science & Innovation Campus, Didcot, UK
4. Division of Structural Biology, Nuffield Department of Medicine, University of Oxford, The Wellcome Centre for Human Genetics, Oxford, UK
5. Oxford University Hospitals NHS Foundation Trust, Oxford, UK
6. Peter Medawar Building for Pathogen Research, Oxford, UK
7. Nuffield Department of Clinical Neurosciences, University of Oxford, Oxford, UK
8. Institute of Global Health, University of Siena, Siena, Brazil; Department of Paediatrics, University of Oxford, Oxford, UK
9. Laboratório de Ecologia de Doenças Transmissíveis na Amazônia, Instituto Leônidas e Maria Deane, Fiocruz, Manaus, Amazonas, Brazil
10. Fundação de Vigilância em Saúde do Amazonas, Manaus, Amazonas, Brazil
11. Laboratorio de vírus respiratórios- IOC/FIOCRUZ, Rio de Janeiro, Brazil
12. Department of Veterinary Integrative Biosciences, Texas A&M University, College Station, TX, United States
13. NIHR Oxford Biomedical Research Centre, Oxford, UK
14. Oxford Vaccine Group, Department of Paediatrics, University of Oxford, Oxford, UK
15. Viral Pseudotype Unit, Medway School of Pharmacy, University of Kent and Greenwich, Chatham Maritime, Kent ME4 4TB, UK
16. Nuffield Department of Medicine, University of Oxford, Oxford, UK
17. MRC Human Immunology Unit, MRC Weatherall Institute of Molecular Medicine, Radcliffe Department of Medicine, University of Oxford, Oxford, UK
18. Jenner Institute, Nuffield Department of Medicine, University of Oxford, Oxford, UK
19. National Infection Service, Public Health England (PHE), Porton Down, Salisbury, UK
20. Translational Gastroenterology Unit, University of Oxford, Oxford, UK
21. Centre For Tropical Medicine and Global Health, Nuffield Department of Medicine, University of Oxford, Oxford, UK
22. Mahidol-Oxford Tropical Medicine Research Unit, Bangkok, Thailand, Department of Medicine, University of Oxford, Oxford, UK

23. South African Medical Research Council, Vaccines and Infectious Diseases Analytics Research Unit, School of Pathology, Faculty of Health Sciences, University of the Witwatersrand, Johannesburg, South Africa
24. Department of Science and Technology/National Research Foundation, South African Research Chair Initiative in Vaccine Preventable Diseases, Faculty of Health Sciences, University of the Witwatersrand, Johannesburg, South Africa
25. Siriraj Center of Research Excellence in Dengue & Emerging Pathogens, Dean Office for Research, Faculty of Medicine Siriraj Hospital, Mahidol University, Thailand
26. Instruct-ERIC, Oxford House, Parkway Court, John Smith Drive, Oxford, UK

# These authors contributed equally to this work.
* corresponding authors
§ Lead contact

Summary

SARS-CoV-2 has undergone progressive change with variants conferring advantage rapidly becoming dominant lineages e.g. B.1.617. With apparent increased transmissibility variant B.1.617.2 has contributed to the current wave of infection ravaging the Indian subcontinent and has been designated a variant of concern in the UK. Here we study the ability of monoclonal antibodies, convalescent and vaccine sera to neutralize B.1.617.1 and B.1.617.2 and complement this with structural analyses of Fab/RBD complexes and map the antigenic space of current variants. Neutralization of both viruses is reduced when compared with ancestral Wuhan related strains but there is no evidence of widespread antibody escape as seen with B.1.351. However, B.1.351 and P.1 sera showed markedly more reduction in neutralization of B.1.617.2 suggesting that individuals previously infected by these variants may be more susceptible to reinfection by B.1.617.2. This observation provides important new insight for immunisation policy with future variant vaccines in non-immune populations.

Introduction

Reports of a severe acute respiratory syndrome in Wuhan China first appeared in December 2019. It was rapidly determined that coronavirus disease 2019 (COVID-19) was caused by infection with a novel beta coronavirus related to the SARS coronavirus and named SARS-CoV-2 (Gorbalenya et al., 2020). SARS-CoV-2 spread rapidly leading to the global pandemic which is still accelerating and has been estimated to have led to 164M infections and 3.4M deaths (https://www.worldometers.info/coronavirus Accessed: 2021-05-17).

Since the first sequence of SARS-CoV-2 was deposited in early January 2020 (Lu et al., 2020), viral genome sequencing efforts have been established in a number of countries to track the evolution of the virus (COG-UK Consortium, 2020). Coronaviruses are large

positive strand RNA viruses and despite some proof-reading capacity (Robson et al., 2020), replication is intrinsically error prone. Progressive mutational change in the virus is therefore inevitable as it undergoes massive numbers of replicative cycles worldwide (Tegally et al., 2021). In particular, changes were anticipated as the virus adapts to its new human host.

Many thousands of mutational changes have been described across the viral genome and whilst most will be detrimental or confer no advantage to the virus, some will be advantageous and be the subject of rapid natural selection (Domingo et al., 2012; Rambaut et al., 2020). Mutations could confer advantage to the virus in a number of ways, but increased transmissibility or escape from innate or acquired immune responses are two potential examples (Volz et al., 2021).

Spike protein (S) is the major surface glycoprotein on coronaviruses. These characteristically trimeric spikes are subdivided into an N-terminal S1 domain responsible for attachment to host cells via its receptor ACE2 (Hoffmann et al., 2020) and a C-terminal S2 domain which is anchored in the viral membrane, cleaved from S1 following cellular attachment and responsible for membrane fusion and cell entry. S1 consists of an N-terminal domain (NTD) followed by the receptor binding domain (RBD) which mediates binding to ACE2, burying ~860 Å of surface area at its tip (Lan et al., 2020).

Analysis of panels of monoclonal antibodies binding to S has led to the identification of a number of potently neutralizing antibodies, some of which have been developed for therapeutic and prophylactic use (Ku et al., 2021; Baum et al., 2020). Antibodies to S2 tend to be poorly neutralizing while potently neutralizing antibodies generally map to S1. Most potent neutralizing antibodies bind the RBD, either on or closely adjacent to the ACE2 interacting

surface and function to block interaction of the virus with ACE2, thereby preventing cellular adhesion and infection (Dejnirattisai et al., 2021; Yuan et al., 2020; Kreye et al., 2020). A second class of potently neutralizing antibodies bind to a site on the NTD termed the supersite, these antibodies do not block interaction with ACE2 and their mode of neutralization is less well understood (Cerutti et al., 2021; Chi et al., 2020; Dejnirattisai et al., 2021).

Many mutations in S have been reported and it appears that the RBD and especially NTD are mutational hotspots (Greaney et al., 2021). The ACE2 interacting surface of S is under intense selective pressure as changes may increase ACE2/RBD affinity, potentially increasing virus transmissibility, whilst the same changes may also reduce antibody binding to the RBD, decreasing the neutralizing potential of immune serum. In late 2020 three variants of concern were identified, B.1.1.7 in the UK, B.1.351 in South Africa and P.1 in Brazil, which rapidly became the dominant variants locally, leading to large second waves of infection and they continue to spread globally. These variants contain changes in the RBD; B.1.1.7 N501Y; B.1.351 N501Y, E484K, K417N and P.1 N501Y, E484K and K417T. These changes increase the affinity of ACE2 to RBD 7-fold for B.1.1.7 and 19-fold for B.1.351 and P.1, which may play a role in increased transmissibility. The neutralizing titres of convalescent and vaccine serum are reduced to the variants with B.1.351 of most concern, leading to a 13-fold reduction in neutralizing titres of convalescent serum with a number of neutralizing monoclonal antibodies completely losing activity (Zhou et al., 2021; Supasa et al., 2021; Dejnirattisai et al., 2021b; Shinde et al., 2021; Madhi et al., 202;Vaccines and Related Biological Products Advisory Committee, 2021; Emary et al., 2021).

There are now at least 15 vaccines authorised for use in one or more countries, and these are designed to elicit antibody (and T-cell) responses to S using S sequences from the original Wuhan virus deposited in January 2020. Vaccines deliver S in a variety of different formats; RNA, viral vectors, recombinant protein or inactivated virus (Krammer, 2020; Polack et al., 2020; Voysey et al., 2020; Baden et al., 2020) (https://www.medscape.com/viewarticle/944933 Accessed: 2021-03-01). Since the S sequence of variant viruses differ from that used for vaccination there is concern that variant viruses may have the potential to evade antibody responses elicited by vaccination. Several studies have now shown that there is reduced vaccine efficacy against mild to moderate disease in countries where B1.351 was dominant (Zhou et al., 2021; Shinde et al., 2021; Madhi et al., 2021, Vaccines and Related Biological Products Advisory Committee, 2021), though protection against severe disease appears to be preserved. Conversely, vaccine efficacy against B.1.1.7 is maintained (Wang et al., 2021; Emary et al., 2021; Supasa et al., 2021).

In this paper we study two variant viruses B.1.617.1 (bearing mutations L452R and E484Q in the RBD) and B.1.617.2 (bearing RBD mutations L452R and T478K) which were first reported from India at the end of 2020 but have spread globally (https://www.gisaid.org/hcov19-variants/) with B.1.617.2 causing particular concern in the UK where it is spreading rapidly and was designated a variant of concern in May 2021. Using a panel of potent neutralizing antibodies, we show that both viruses show partial or complete escape from neutralization by some antibodies but that neutralization of most monoclonal antibodies is unaffected. Neutralization by a panel of plasma collected from convalescent cases from the UK early in the pandemic show 4-fold and 2.7-fold reduction in neutralization titres to B.1.617.1 and B.1.617.2 respectively, compared to an early Wuhan related strain.

There are also significant reductions in neutralization titres of sera collected from recipients of the Oxford-AstraZeneca and Pfizer-BioNTech vaccines but no evidence of widespread complete escape from neutralization. We also look at the ability of sera from individuals infected with B.1.1.7, B.1.351 and P.1 to neutralize B.1.617.1 and B.1.617.2 and find that a sizeable number of sera from B.1.351 and P.1 fail to neutralize B.1.617.2. Finally, we measure the affinity of B.1.617.1 and B.1.617.2 RBDs for ACE2, showing a modest increase in affinity compared to the Wuhan RBD sequence, use structural information to identify the mechanism of escape from monoclonal antibodies and perform a simple analysis of antigenic distances between variants to illustrate the emerging antigenic landscape of SARS-CoV-2.

Results

The B.1.617 lineage

There are three sub-lineages of B.1.617: B.1.617.1, B.1.617.2 and B.1.617.3. B.1.617.3 was the first to be identified in India in October 2020 and is now relatively uncommon. B.1.617.1 and B.1.617.2 variants are now found across most of the globe including the UK where they have become the second and third-most widespread variants of concern respectively according to COG-UK data (COG-UK, Consortium, 2020) (**Figure 1A**). B.1.617.2 in particular has risen to dominate the sequenced genomes in the week around 4th June, replacing the B.1.1.7 strain. B.1.617.1 sequences deposited on GISAID (https://www.gisaid.org/hcov19-variants/) are highly variable but contain the RBD mutations L452R and E484Q at the periphery of the ACE2 interacting surface, together with P681R (which may increase furin cleavage of S1), the S2 mutation Q1071H and up to three NTD substitutions: T95I, G142D and E154K (**Figure 1B**). E484Q is a mutation at the same position as E484K seen in the B.1.351 and P.1 variants, although the change in physico-chemical properties is less for the glutamine than the lysine sidechain (Zhou et al., 2021; Dejnirattisai et al., 2021b). B.1.617.2 (**Figure 1C**) exhibits RBD mutations L452R and T478K, T19R, G142D R158G and A222V substitutions, together with a double deletion

(156-157) in the NTD and S2 substitution D950N. B.1.617.2 shares L452R and P681R with B.1.617.1, and 20% of reported sequences share T95I. L452R has also been identified in B.1.427 and B.1.429 (Deng et al., 2021) and T478K is found in B.1.1.519. Unlike B.1.617.1, B.1.617.2 contains NTD deletions which matches a general trend of SARS-CoV-2 variants reducing the size of the NTD.

Neutralization of B.1.617.1 and B.1.617.2 by a panel of potently neutralizing antibodies

We have previously reported the generation of a large panel of 377 human monoclonal antibodies generated from patients who had recovered from SARS-CoV-2 infection early during the pandemic (Dejnirattisai et al., 2021a). The twenty most potent neutralizing antibodies (FRNT50 <0.1μg/ml) were selected for these studies, 19 bind RBD and block interaction with ACE2, while the last, mAb-159, binds to the NTD. We used a pseudotyped lentivirus to measure neutralization of B.1.617.1 (Temperton, 2010) and a live viral isolate to measure neutralization of B.1.617.2. Neutralization of viral variants was compared to neutralization of Victoria (SARS-CoV-2/human/AUS/VIC01/2020), a Wuhan related strain isolated early in the pandemic from Australia (Caly et al., 2020; Seemann et al., 2020).

For B.1.617.1, 8 mAb: 58, 88, 170, 278, 281, 316, 384 and 398 showed a >5-fold reduction in neutralization titres with most of these showing an almost complete knock out of activity (**Figure 2A, Table S1**). Neutralization of B.1.617.2 virus, which shares the L452R RBD mutation with B.1.617.1 was measured using a focus reduction neutralization test (FRNT) and compared to the Victoria viral isolate. Neutralization of B.1.617.2 was reduced >5-fold for 6 antibodies, neutralization by the NTD mAb159 was completely lost, whilst neutralization by mAbs: 58, 170, 278, 281 and 384 was reduced in common with neutralization of B.1.617.1,

suggesting that these antibodies may share an epitope overlapping the RBD L452R substitution. Interestingly, mAb 253 showed increased neutralization of B.1.617.2.

To confirm the role of the L452R RBD mutation we tested mAb neutralization with a B.1.429 pseudotyped lentivirus (containing the single L452R substitution in RBD), which showed reduced neutralization with mAb 58, 170, 278, 281 and 384. Finally, we performed neutralization assays on a pseudotyped lentivirus expressing B.1.1.519 S, which contains the single T478K substitution in the RBD and saw no significant changes in neutralization (**Figure S1, Table S1**).

Neutralization of B.1.617.1 and B.1.617.2 by monoclonal antibodies developed for clinical use.

A number of potent monoclonal antibodies are being developed for clinical use and some have received emergency use authorisation (Ku et al., 2021; Baum et al., 2020; Kemp et al., 2021). We performed neutralization assays against B.1.617.1 and B.1.617.2 using antibodies S309 Vir (Pinto et al., 2020), AZD8895, AZD1061 and the combination AZD7442 AstraZeneca, REGN10987 and REGN10933 Regeneron, LY-CoV555 and LY-CoV16 Lilly and ADG10, ADG20 and ADG30 from Adagio (**Figure 2B, Table S1**). Potent activity was maintained on B.1.617.1 and B.1.617.2 with small, up to 5-fold, reductions in neutralization for some antibodies. The exceptions were LY-CoV555, which completely failed to neutralize B.1.617.1 and was severely reduced on B.1.617.2 (Greaney et al., 2021), and for unknown reasons S309 (Pinto et al., 2020) could not neutralize the Victoria pseudotyped virus so we could not reliably compare its activity on B.1.617.1.

Binding of B.1.617.1 and B.1.617.2 RBD to ACE2 and mAb

To understand the contribution of interactions at the RBD to the properties of the two variants we analysed interactions of variant RBDs with ACE2 and the panel of neutralising antibodies using biolayer interferometry. The results for ACE2 (**Figure 3A**) show that both the B.1.617.1 and B.1.617.2 double mutations (L452R and E484Q, and L452R and T478K) show perhaps a modest increase in affinity for ACE2 (25 and 57 nM respectively) compared to Victoria RBD (75 nM). B.1.1.519 (T478K) has a similar K_D (33 nM), suggesting that L452R does not significantly alter affinity for ACE2.

The results for antibody binding to RBDs mirror the neutralisation results for both B.1.617.1 and B.1.617.2 (**Figure 3B,C**). It will be seen, as expected, that the antibodies affected are proximal to the mutation sites. The antibodies most affected are especially in the top and front in the neck epitope (nomenclature of (Dejnirattisai et al., 2021a)), with a small impact on some antibodies belonging to the right flank epitope. The reasoning presented above for the assignment of individual mutations to effects on antibody potency is consistent with the site of antibody attachment.

Structural solution for antibody escape

We performed three exemplar structural analyses to test our understanding of the physicochemical basis of antibody escape. Firstly, we determined the crystal structure (at 2.3 Å resolution) of Fab 278 in complex with Victoria RBD and Fab 222 (Methods, **Figure 4A-D**, **Table S2**). Neutralisation and binding of of mAb 278 are affected for both B.1.617.1 and B.1.617.2 and we inferred that the mutation of RBD residue 452 was responsible. The structure confirms that neither RBD residue 478 nor 484 contact the antibody and binding abrogation is mediated by direct contact between the 16-residue long HC CDR3 and RBD residue 452, which could not accommodate the major increase in sidechain size in going from

leucine to arginine in the variant viruses (**Figure 4C)**. We note that although REGN10987 and mAb 75 bind at a similar site to mAb 278 and all three antibodies overlap the ACE2 binding site (Baum et al., 2020; Dejnirattisai et al., 2021a) the engagement is sufficiently different that neither REGN10987 nor mAb 75 directly contact RBD residue 452 (**Figure S2**) REGN10987 is effective against both B.1.617.1 and B.1.617.2, whilst mAb 75 is a weak binder). In fact, of the 13 different Fab complexes we have structures for, only mAb 278 makes strong contacts with RBD residue 452, however in addition mAb 384 makes weak contacts with RBD residue 452 (**Figure 4E,F**), but more important contacts with residue 484. However, we note that McCallum et al. (McCallum et al., 2021) report several RBD residue 452 interacting antibodies and in our set of 20 potent neutralisers we have inferred interaction from the neutralization and binding data for three further mAbs, 58, 170 and 281 for which we do not have structures but competition mapping positioning is consistent with contact (**Figure 3B**) (Dejnirattisai et al., 2021a), suggesting that such antibodies are not uncommon in responses to infection with Victoria-like viruses.

Secondly, we determined the crystal structure of a ternary complex of RBD-L452R with Fabs 253 and 75 (Methods, **Figure 4G** and **Table S1**). The RBD 452 mutation had no effect on neutralization or binding of mAb 253 and the structure confirms that the RBD L452R mutation introduces no significant change in the RBD structure and residue 452 does not directly contact Fab 253 (**Figure 4G**). The third crystal structure determined is closely related, it is a ternary complex of Fab 253 with RBD-T478K and Fab 45 (**Figure 4H, Table S2**). Fab 253 is the only antibody whose binding is significantly perturbed by the mutation at RBD residue 478 (the closely related mAb 55 shows a similar but reduced effect) and the mutation to lysine actually increases neutralisation titre by approximately one log. Perhaps surprisingly this is the only example we have come across of a marked increase in binding to

a variant virus and the structure confirms that this effect is due to direct interaction with RBD residue 478, with the lysine side chain in the variant RBD folding away behind the CDR1 loop of the LC (**Figure 4I,J**). In addition, comparison of the overall mode of engagement of mAb 253 between the two differently mutated RBDs reveals that the 478 mutation induces a modest change in the pose of the antibody (**Figure 4I**). It is perhaps surprising that the threonine to lysine mutation of RBD residue 478, which represents a marked change in size and charge has no deleterious effect on the binding of any of our set of potent monoclonal antibodies. This suggests that antibody response against Victoria-like viruses do not include a significant number of potent neutralising antibodies that bind in this region, perhaps because this residue is towards the back of the left shoulder facing away from the area where ACE2 attaches. Nevertheless, this residue is extremely exposed and it is possible that responses in people infected by B.1.351 may produce a significant number of antibodies that interact with mutated RBD residue 484 some of which are likely to be sensitive to the mutation of RBD residue 478, perhaps contributing to the considerable antigenic distance between B.1.351 and B.1.617.2.

Finally, by reference to structures we have determined previously we can confirm that antibody 316, which only loses neutralization of B.1.617.1 contacts the B.1.617.1 specific mutation E484 but not RBD residues L452 or T478 (**Figure 4K,L**).

Neutralization of B.1.617.1 by convalescent serum

Deposited B.1.617.1 sequences are highly variable (COG-UK Consortium, 2020), so we constructed pseudoviruses containing three different B.1.617.1 S sequences. Compared to Wuhan sequence, all share L452R and E484Q in the RBD together with D614G and P681R which are the only substitutions in B.1.617-C; B.1.617-A has in addition E154K in the NTD,

plus E1072K and V1176F in S2; B.1.617-B contains T95I, G142D, E154K, in the NTD and Q1071H in S2 (**Figure 1B**).

We collected 4-9 week convalescent plasma from individuals infected during the first wave of infection in the UK before June 2020, plasma from individuals infected with B.1.1.7 in the UK (n=18) confirmed by sequence or S-gene knock out in diagnostic PCR), serum from cases of P.1 (n=17 sequence confirmed) collected in Brazil and serum from cases of B.1.351 collected from the UK and South Africa (n=14) sequence confirmed n=12, or isolated contacts of sequence confirmed cases who developed infection during quarantine n=2) (Dejnirattisai et al., 2021a; Supasa et al., 2021; Zhou et al., 2021; Dejnirattisai et al., 2021b).

Neutralization of B.1.617.1 pseudoviruses were compared to neutralization of Victoria (Caly et al., 2020) using the UK samples taken in early 2020 (**Figure 5A,B, Table S3**) (Dejnirattisai et al., 2021a). Relative to Victoria, geometric mean neutralization titres were reduced 2.5 fold ($p=0.0002$) for B.1.617-A, 3.9-fold ($p<0.0001$) for B.1.617.1-B and 1.5-fold ($p=0.0248$) for B.1.617-C. Differences in neutralization of three different B.1.617.1 subtypes may be due to mutations occurring in the NTD, 0 in B.1.617.1-C, 1 in B.1.617.1-A and 3 in B.1.617-B which was the most difficult to neutralize. B.1.617-B was used for subsequent experiments.

Next, we measured neutralization of B.1.617.1-B compared to Victoria by sera taken from cases infected with B.1.1.7, 4.3-fold reduction ($p<0.0001$), B.1.351, 1.8-fold reduction ($p=0.0833$) and P.1, 2.1-fold reduction ($p=0.0026$), indicating that infection with these variant viruses provides substantial cross protection against B.1.617.1 with no samples showing complete escape from neutralization (**Figure 5C-E, Figure S3**).

Neutralization of B.1.617.2 by convalescent serum

We measured neutralization of B.1.617.2 native virus on the same set of UK convalescent samples taken early during the pandemic (**Figure 6A, Figure S4, Table S3**). Compared to Victoria geometric mean titres for B.1.617.2 were reduced 2.7-fold ($p<0.0001$). Compared to Victoria, neutralization titres to B.1.617.2 were reduced for B.1.1.7 serum 2.8-fold ($p=0.0003$); for B.1.351 serum 6.0-fold ($p<0.0001$) and for P.1 serum, 2.9-fold ($p=0.0005$) (**Figure 6B-D, Table S3**).

To get an idea of how people previously infected with B.1.1.7, B.1.351 and P.1 were protected from B.1.617.2, we compared the neutralization titres to B.1.617.2 to the neutralization of the homologous infecting lineage. For B.1.1.7 serum neutralization of B.1.617.2 was 1.5-fold reduced ($p=0.4038$) compared to B.1.1.7, for B.1.351 serum neutralization was 11.6-fold reduced ($p=0.0001$) compared to B.1.351 and for P.1 was 11.3-fold reduced ($p<0.0001$) compared to P.1 **(Figure 6B-D)**.

Serum from donors infected with B.1.1.7 appears to give good protection against all variants of concern whereas, protection from B.1.617.2 afforded by previous infection with B.1.351 and P.1 is much more compromised. Inspection of the neutralization curves using B.1.351 and P.1 serum (**Figure 6E,F**) show that in many cases neutralization is almost completely lost to B.1.617.2, most profoundly for P.1, suggesting that individuals infected with B.1.351 and P.1 may be at risk of reinfection with B.1.617.2.

Protection from B.1.617.1 and B.1.617.2 by vaccine serum

We tested neutralization of B.1.617.1 and B.1.617.2 using serum from individuals who had received 2 doses of the BNT162b2 Pfizer-BioNTech or ChAdOx1 nCoV-19 Oxford-

AstraZeneca vaccine (Polack et al., 2020; Voysey et al., 2020). For Pfizer-BioNTech, serum was collected 4–14 days following the second dose of vaccine administered 3 weeks after the first dose (n=25). For the Oxford-AstraZeneca vaccine, serum was taken 14 or 28 days following the second dose, administered 8–14 weeks following the first dose (N=25). Geometric mean neutralization titres against B.1.617.1 were reduced 2.7-fold ($p<0.0001$) relative to the Victoria virus for the Pfizer-BioNTech vaccine serum (**Figure 7A, Figure S5, Table S3**) and 2.6-fold ($p<0.0001$) for the Oxford-AstraZeneca vaccine (**Figure 7B**). For B.1.617.2 titres were reduced 2.5-fold ($p<0.0001$) relative to the Victoria virus for the Pfizer-BioNTech vaccine serum (**Figure 7C**) and 4.3-fold ($p<0.0001$) for the Oxford-AstraZeneca vaccine (**Figure 7D**). For B.1.617.2 reductions were comparable to those seen with B.1.1.7 and P.1 (Supasa et al., 2021; Dejnirattisai et al., 2021b) with only a small number of samples failing to reach FRNT50 titres at 1:20 serum dilution in contrast to the results seen for neutralization of B.1.351 (**Figure S4**).

Finally, we performed neutralization assays using sera from volunteers 4 (n=20) and 10 weeks (n=20) after a single dose of the Pfizer-BioNTech vaccine. In the UK for both Oxford-AstraZeneca and Pfizer-BioNTech vaccines a dosing interval of 12 weeks has been recommended to achieve higher vaccine coverage. Following one dose of vaccine neutralization of Victoria was observed in most individuals with FRNT≥50% in 16/20 at 4 weeks and 9/20 at 10 weeks. Titres against B.1.617.2 were lower with FRNT≥50% in 4/20 at 4 weeks and 0/20 at 10 weeks (**Figure 7E, F**). Peak neutralization titres at serum dilution 1/20 were an average of 63% and 47% for Victoria and 27% and 7% for B.1.617.2 at 4 and 10 weeks respectively, with many of the 10 week samples showing no evidence of neutralization of B.1.617.2 (**Figure 7G, H**).

The antigenic landscape of the present major variants

To visualise and quantify the emerging antigenic landscape of SARS-CoV-2 we devised a method related to antigenic cartography (Smith et al., 2004; Fonville et al., 2014). We define 'antigenic distance' by comparison of the log of dilution values for 50% neutralisation for all the available serum/virus strain pairs (Dejnirattisai et al., 2021a; Supasa et al., 2021; Zhou et al., 2021; Dejnirattisai et al., 2021b). Three principal axes of variation determined by single value decomposition of this serum/virus strain matrix were displayed to show the distribution of the strains in antigenic space. The result, using the somewhat incomplete set of data available from our studies is shown in (**Figure 7I, Supplementary Video 1**). This provides a very simple view onto complex, sparse and noisy data and confirms the inferences made above, that the largest distance is between the B.1.351/P.1 lineages and B.1.617.2, whereas B.1.617.1 is significantly closer to B.1.351/P.1. Whilst B.1.351 is roughly orthogonal to B.1.617.2, P.1 is essentially opposite (anticorrelated with) B.1.617.2, reflecting the especially poor ability of P.1 serum to neutralise B.1.67.2. Note that both B.1.1.7 and Victoria are reasonably central to the distribution.

Discussion

The inevitable evolution of SARS-CoV-2 following its zoonotic transfer to humans in Wuhan in late 2019 prompted the establishment of sequencing efforts such as COVID-19 genomics UK (COG-UK) (COG-UK Consortium, 2020). SARS-CoV-2 genome surveillance in many parts of the world was slow to start and there are many regions where surveillance is either absent or completely underpowered compared with the scale of infections. It is likely that the true scale of the diversity in SARS-CoV-2 is underestimated and that further concerning variants are circulating and will continue to arise. Early in the pandemic SARS-CoV-2 was under selective pressure to adapt to its new host, to evade the innate immune system, to

efficiently bind to and infect target cells and to transmit to the next host. As the population develops immunity, by either natural infection or vaccination, pressure is mounting to select mutations that allow the virus to more effectively find an infectible host through increased transmissibility, or to evade the acquired immune response and cause reinfection.

Since the S protein is intimately involved in the initiation of infection and is the target of neutralizing antibody responses it is no surprise that it is evolving rapidly and that changes in S likely underpin some of the phenotypes expressed by variants of concern. S is a large protein >1200 amino acids but a very small 25 amino acid patch at its apex, mediating RBD/ACE2 interaction, is key. Mutations in and around the ACE2 interacting surface are found in all the variants of concern B.1.1.7, B.1.351, P.1 as well as the three B.1.617 sub-lineages (**Figure 7H**).

In this report we have measured the affinities for B.1.617.1 (L452R, E484Q), B.1.617.2 (L452R, T478K), and B.1.1.519 (T478K) RBDs for ACE2. These results show a very modest increase (less than 2-fold) in affinity for the variants. In contrast, we have previously measured the affinities of B.1.1.7 (N501Y), B.1.351 (N501Y, E484K, K417N) and P.1 (N501Y, E484K, K417T) RBDs for ACE2 and found more marked (7, 19 and 19-fold increases in affinity respectively compared to Wuhan RBD), which may be driving the increased transmissibility of these strains. In line with our results Schreiber et al., (Zahradník et al., 2021) find that none of the three B.1.617 RBD mutations were selected by forced *in vitro* evolution to optimise ACE2 binding. It is likely therefore that the B.1.617.1 and B.1.617.2 RBD mutations were selected by different pressure. Nevertheless, the *in vitro* evolution experiments demonstrated that the increases in RBD/ACE2 affinity seen in today's variants of concern are far from the limits that can be achieved, so in the future more radical

antigenic variation, which would render the virus unfit by reducing affinity for ACE2 might be rescued by employing these ACE2-binding enhancing mutations.

A hotspot for S sequence change is the NTD with multiple changes occurring in tandem consisting of amino acid substitutions together with small deletions and insertions. The NTD is the site of binding of a number of potently neutralizing antibodies whose mode of action is not yet fully understood since unlike most potent anti-RBD antibodies they do not block ACE2 interaction (Cerutti et al., 2021). B.1.617.2 has a highly mutated NTD (T19R, G142D, Δ156-157, R158G, A222V) which would be predicted to disrupt the so-called "super site" on the NTD mediating neutralization (Cerutti et al., 2021) (**Figure S2**), and in line with this the neutralizing activity of mAb 159 which binds to the mutated area is completely lost on B.1.617.2. B.1.617.1 sequences are quite variable and here we examined three different isolates with 0, 1 or 3 mutations in the NTD, with the version containing 3 mutations being the most resistant to neutralization by convalescent plasma (**Figure 1B, Figure S2**).

Mutations L452R and E484Q knocked out activity of several potently neutralizing antibodies that bind to the RBD but T478K, despite being relatively close in space to other key residues such as 484 did not appear to have a negative effect on any of the panel of potent neutralisers. We have solved the structure of a complex of RBD with mAb 278 and confirm that this antibody contacts L452 (**Figure 4A**) explaining its loss of activity on B.1.617.1 and B.1.617.2. Furthermore, structures of other antibodies such as 384 demonstrate reliance on contacts with L452 and E484 with the contacts with E484 probably dominant to L452 (**Figure 4L**). On the other hand, the structure of mAb 316 shows contact with E484 but no contact with L452 (**Figure 4J**). The light chain of mAb 253 contacts RBD residue T478 and the change at 478 enhances the binding/neutralization of B.1.617.2 (**Figure 4G,H**).

Because of the loss of activity of some potent neutralizing mAbs we expected to see a reduction in neutralization of B.1.617.1 and B.1.617.2 by convalescent and vaccine serum. For B.1.617.1 we saw reductions of 3.9-fold for convalescent plasma, 2.7-fold for the Pfizer-BioNTech vaccine and 2.6-fold reduction for the Oxford-AstraZeneca vaccine and for B.1.617.2 reductions were 2.7, 2.5 and 4.3-fold respectively. Reductions were comparable in scale with those seen with B.1.1.7 and P.1 with no evidence of widespread escape from neutralization, in contrast to that seen with B.1.351. It would seem likely from these results that the current RNA and viral vector vaccines will provide protection against the B.1.617 lineage, though an increase in breakthrough infections may occur as a result of the reduced neutralizing capacity of sera. Given the apparent high transmissibility of the variants, immunization of those at highest risk (older adults and those with co-morbidities) globally with at least one dose of the current generation of vaccines is urgently needed. It is known that the proportion of the population with strong neutralizing activity increases with a second dose (Folegatti et al., 2020) and we find that following a single dose of Pfizer-BioNTech vaccine neutralisation neutralization of B.1.617.2 is limited. Administration of two doses for those at greatest risk will therefore be needed to prevent infection. Of interest, infection with B.1.1.7 seems to provide reasonable cross-protection against all variants of concern, which means B.1.1.7 might be a candidate for new variant vaccines to provide the broadest protection.

Of more concern, was the neutralization of B.1.617.2 by sera from people previously infected with B.1.351 and P.1, with 4/14 and 10/17 showing a complete absence of neutralization of B.1.617.2 respectively. Although in some cases neutralization was knocked out for B.1.617.2 some sera showed almost no change in neutralization between B.1.315 or P.1 and the Victoria

strain, understanding at an epitope level how sera from these individuals differentially recognise variant viruses will be interesting to determine. These results suggest that there is a risk of reinfection with B.1.617.2 in individuals previously infected by variants B.1.351 and P.1.

An explanation for the disparity in neutralization of B.1.617.2 by B.1.351 and P.1 serum may be that the differences between the two viruses are additive. Thus, there are three RBD amino acid substitutions in B.1.351 and P.1 compared to Wuhan RBD, but five compared to B.1.351 and P.1 (the amino acid before the number represents the B.1.617.2 RBD sequence: K417N/T, R452L, K478T, N501Y, E484K). In addition, there are the multiple differences in the NTDs, meaning that many antibodies generated by B.1.351 or P.1 infection will likely be ineffective against B.1.617.2. In B.1.617.1 there are 4 changes relative to B.1.351 and P.1, K417N/T, L452R, N501Y, Q484K and it may be that lessening of the charge difference in RBD residue Q484K vs E484K and less pronounced differences in the NTDs make B.1.617.1 less resistant to neutralization by B.1.351 and P.1 serum. However as more variants emerge and robust serological data such as those presented here are obtained then it becomes essential to visualise and quantify the antigenic landscape of SARS-CoV-2 rather than rely on such. increasingly complicated, narrative explanations. We present such a method (**Figure 7J, Video S1**), related to those termed antigenic cartography. We define a multidimensional antigenic space representing ‘antigenic distances’ within the sero-complex and show that even using the incomplete data available projecting the principle components into to a lower-dimensional space allows visualisation of the antigenic relationships between the different lineages, confirming the qualitative assessment that the largest distance is between B.1.617.2 and the B.1.351/P.1 lineages (with P.1 being essentially anti-correlated with B.1.617.2), whereas B.1.617.1 is significantly closer to B.1.351/P.1. We suggest that the virus closest to

the centroid of the distribution of antigenic differences might be a natural candidate for a vaccine antigen able to produce the most effective responses against all currently identified variants (in this case it would be Wuhan or B.1.1.7). Useful extensions of the method might be to take account not only antigenic distance, but also the nature and levels of the antibody responses against each virus. One striking outcome of this analysis is that clustering variants on the basis of antigenic distance gives completely different results from clustering by lineage, reflecting the major effect of a small number of mutations, which almost entirely switch the electrostatic properties by introducing basic residues around the edge of the ACE2 binding footprint on the RBD (**Figure 7J**).

The results showing reduced neutralization ability of serum derived from B.1.351 and P.1 individuals should drive consideration of policy decisions with new variant vaccines, when available, as it may indicate that the original "Wuhan" vaccine might be better than a B.1.351 vaccine for naïve populations even in areas where B.1.351 is the dominant variant. As SARS-CoV-2 virus continues to diverge antigenically consideration is being given to booster vaccines to give further protection against viral variants such as B.1.351. How effective boosting will be to redirect the response towards the variants from the initial prime with Wuhan is to be determined. However, it is becoming more likely that more than one variant will be required to provide protection as the SARS-CoV-2 sero-complex continues to evolve, we suggest that one component will likely continue to include Wuhan related strains or B.1.1.7 as, for now at least, they appear to be more centrally positioned in the sero-complex, able to provide protection against multiple viral variants.

Finally, we show a 1.34-fold reduction between 4 and 10 weeks in neutralization titres to Victoria in individuals given a single dose of the Pfizer-BioNTech vaccine and almost

complete absence of neutralization of B.1.617.2 at 10 weeks. Previous studies have shown protection following a single dose of vaccine despite low or absent antibody responses, but recently in the UK some reduction in Pfizer-BioNTech effectiveness has been detected at 10 weeks (https://assets.publishing.service.gov.uk/government/uploads/system/uploads/attachment_data/file/988193/Vaccine_surveillance_report_-_week_20.pdf), presumably as a result of waning immunity, leading to the recommendation that the second vaccine dose interval should be reduced from 12 to 8 weeks in those over age 50 (https://www.gov.uk/government/news/jcvi-advice-to-mitigate-impact-of-b1-617-2-variant).

In summary, we report an in-depth study of antibody binding and neutralization of B.1.617.1 and B.1.617.2 viruses. Although there is reduction in neutralization titres using convalescent or vaccine sera there is no evidence of widespread escape suggesting that the current generation of vaccines will provide protection against the B.1.617 lineage, although reduced titres may lead to some breakthrough infections. However, there is a concern that some unvaccinated individuals previously infected with B.1.351 and P.1 may be more at risk of reinfection with B.1.617.2. Further epidemiological data are needed to assess whether breakthrough infections following escape mutations are common, and whether they will progress to severe disease and hospitalisation. If this escape from the neutralising capacity of vaccines continues with evolution of new variants in vaccinated populations, and leads to a substantial reduction in effectiveness against hospitalisation, there will be a significant impact on attempts to alter the course of the pandemic through immunisation and an urgent need to revise immunogens.

Limitations of the study

We have compared pseudoviral neutralization data with live virus data, which is not ideal as some pseudoviral constructs did not recapitulate neutralization live virus assays for monoclonal antibodies and we believe that live virus assays are preferable when available.

The in vitro neutralization assays described here are performed in the absence of complement or Fc-receptor bearing cells, that can mediate antibody dependent cell mediated cytotoxicity meaning they may underestimate the protection of immune serum. Assays do not measure the T cell response which may contribute to protection from severe disease and appear less disrupted by the changes present in the variants of concern (Skelly et al., 2021). In the next few weeks through careful studies in the UK it will become clear how effective vaccines are at preventing B.1.617 infection and transmission and crucially, progression to severe disease.

Further investigation of the antibody response in individuals infected with B.1.351 and P.1 is warranted to understand the complex cross protective responses between different sera and variants, it will be particularly interesting to see how much the epitopes of neutralizing antibodies are skewed by infection with B.1.351 and P.1. Finally, the mechanism of neutralization of antibodies binding to the NTD and dissection of the role that antibodies to the NTD make to neutralization is worthy of further investigation.

Acknowledgements

This work was supported by the Chinese Academy of Medical Sciences (CAMS) Innovation Fund for Medical Science (CIFMS), China (grant number: 2018-I2M-2-002) to D.I.S. and G.R.S. H.M.E.D. and J.Ren are supported by the Wellcome Trust (101122/Z/13/Z), Y.Z. by Cancer Research UK (C375/A17721), D.I.S. and E.E.F. by the UKRI MRC (MR/N00065X/1), and NT by the MRC (MC_PC_19060 and MC_PC_20016) and the

Wellcome Trust (GB-CHC-210183). D.I.S. and G.R.S. are Jenner Investigators. We are also grateful for a Fast Grant from Fast Grants, Mercatus Center to support the isolation of human monoclonal antibodies to SARS-CoV-2, Schmidt Futures for support of this work. This is a contribution from the UK Instruct-ERIC Centre. The Wellcome Centre for Human Genetics is supported by the Wellcome Trust (grant 090532/Z/09/Z). F.G.N. is a CNPq fellow and is supported by FAPEAM (PCTI-EmergeSaude/AM call 005/2020 and Rede Genomica de Vigilancia em Saude - REGESAM), Conselho Nacional de Desenvolvimento Cientıfico e Tecnologico (grant 403276/2020-9), and Inova Fiocruz/ Fundac¸ao Oswaldo Cruz (Grant VPPCB-007-FIO-18-2-30 - Gerac¸ao de conhecimento). SJD is funded by an NIHR Global Research Professorship (NIHR300791). Virus used for the neutralisation assays was isolated by Julian Druce, Doherty Centre, Melbourne, Australia. Chanice Knight, Emily Chiplin, Ross Fothergill and Liz Penn contributed to assays. We acknowledge Diamond Light Source for time on Beamline I03 under Proposal lb27009 for COVID-19 Rapid Access. Huge thanks to the teams, especially at the Diamond Light Source and Department of Structural Biology, Oxford University that have enabled work to continue during the pandemic. The computational aspects of this research were supported by the Wellcome Trust Core Award Grant Number 203141/Z/16/Z and the NIHR Oxford BRC. The Oxford Vaccine work was supported by UK Research and Innovation, Coalition for Epidemic Preparedness Innovations, National Institute for Health Research (NIHR), NIHR Oxford Biomedical Research Centre, Thames Valley and South Midland's NIHR Clinical Research Network. We thank the Oxford Protective T-cell Immunology for COVID-19 (OPTIC) Clinical team for participant sample collection, the Oxford Immunology Network Covid-19 Response T cell Consortium for laboratory support and Red Avenue Foundation for their support. We acknowledge the rapid sharing of Victoria, B.1.1.7 and B.1.351 which was isolated by scientists within the National Infection Service at PHE Porton Down, and the B.1.617.2 virus was kindly provided Wendy

Barclay and Thushan De Silva. We thank The Secretariat of National Surveillance, Ministry of Health Brazil for assistance in obtaining P.1 samples. This work was supported by the UK Department of Health and Social Care as part of the PITCH (Protective Immunity from T cells to Covid-19 in Health workers) Consortium, the UK Coronavirus Immunology Consortium (UK-CIC) and the Huo Family Foundation. EB and PK are NIHR Senior Investigators and PK is funded by WT109965MA and NIH (U19 I082360). DS is an NIHR Academic Clinical Fellow. The team at the University of Witwatersrand were supported by The Bill & Melinda Gates Foundation (grant number INV-016202). The views expressed in this article are those of the authors and not necessarily those of the National Health Service (NHS), the Department of Health and Social Care (DHSC), the National Institutes for Health Research (NIHR), the Medical Research Council (MRC) or Public Health, England.

Author Information

These authors contributed equally: CL, HMG, AT, DZ, PS, WD, AJM.

Contributions

D.Z. performed BLI interaction analyses. D.Z., J.R., T.S.W., N.G.P., M.A.W. and D.R.H. prepared the crystals, enabled and performed X-ray data collection. J.R., E.E.F., H.M.E.D. and D.I.S. analysed the structural results. G.R.S., J.M., P.S., Y.Z., D.Z., B.W., R.N., A.T., J.S-C., C.L-C. and C.L. prepared the Spike constructs, RBDs, ACE2 and antibodies and, W.D. and P.S. performed neutralization assays. D.C. and N.T. provided materials. H.M.G. wrote MABSCAPE and performed mapping and cluster analysis, including sequence and antigenic space analyses. S.A.C.C., F. G. N., V.N., F. N., C. F.D.C., P.C.R., A.P-C., M.M.S., A.J.M., E.B., S.J.D., D.S., C.D., T.D., A.J.P., J.C.K., P.K., M.W.C., T.L., S.B., A.F., M.B., S.B-R., E.C. and S.C.G. S.J., T.G.R.,C.M.,T.M., P.G, N.S.,Z.D.,K.D.S, M.C.N., S.M. assisted with

patient samples and vaccine trials. E.B., M.W.C., S.J.D., P.K. and D.S. conceived the study of vaccinated healthcare workers and oversaw the OPTIC Healthcare Worker study and sample collection/processing. V.B. performed molecular testing and sequencing, G.R.S. and D.I.S. conceived the study and wrote the initial manuscript draft with other authors providing editorial comments. All authors read and approved the manuscript.

Competing Financial Interests

GRS sits on the GSK Vaccines Scientific Advisory Board. Oxford University holds intellectual property related to the Oxford-AstraZeneca vaccine. AJP is Chair of UK Dept. Health and Social Care's (DHSC) Joint Committee on Vaccination & Immunisation (JCVI) but does not participate in the JCVI COVID19 committee, and is a member of the WHO's SAGE. The views expressed in this article do not necessarily represent the views of DHSC, JCVI, or WHO. The University of Oxford has entered into a partnership with AstraZeneca on coronavirus vaccine development. The University of Oxford has protected intellectual property disclosed in this publication. S.C.G. is co-founder of Vaccitech (collaborators in the early development of this vaccine candidate) and is named as an inventor on a patent covering use of ChAdOx1-vectored vaccines and a patent application covering this SARS-CoV-2 vaccine (PCT/GB2012/000467). T.L. is named as an inventor on a patent application covering this SARS-CoV-2 vaccine and was a consultant to Vaccitech for an unrelated project during the conduct of the study.

Figures

Figure 1. Mutational landscape of B.1.617 lineage. (A) Evolution plot showing trajectories of various mutations in the COG-UK data. Certain mutations were used to select for sequences typically belonging to a given strain: 501Y and Δ69 to select the B.1.1.7 variant,

501Y, 484K and 417N to select the B.1.351 variant, 501Y, 484K and 417T to select the P.1 variant, E484Q and L452R to select the B.1.617.1 variant and T478K and L452R to select the B.1.617.2 variant. (B-C) Schematic showing the locations of amino acid substitutions in B.1.617.1 (B) and B.1.617.2 (C) relative to the ChAdOx1 SARS-CoV-2 sequence as drawn in previous studies (Dejnirattisai et al., 2021a; Supasa et al., 2021; Zhou et al., 2021; Dejnirattisai et al., 2021b), with all amino acid mutations above 5% explicitly labelled. Mutations coloured in bold were included in the constructs used in this study for the given strain. Under the structural cartoon is a linear representation of S with changes marked for B.1.617.2 live virus and the three sub-variants of B.1.617.1 (a, b, c) used in this study are detailed. Where there is a charge change introduced by mutations the change is coloured (red if the change makes the mutant more acidic/less basic, blue more basic/less acidic).

Figure 2. Neutralization of B.1.617.1 and B.1.617.2 by monoclonal antibodies. (A) Neutralization of B.1.617.1-B and B.1.617.2 by a panel of 20 potent human monoclonal antibodies and candidate therapeutic antibodies. Neutralization of B.1.617.1-B as measured by pseudovirus assay is shown as open triangles and neutralization of B.1.617 virus as measured by FRNT is shown as closed circles, comparison is made with neutralization curves for Victoria that we have previously generated (Supasa et al., 2021). Neutralization titres are reported in **Table S1**. (B) Shows equivalent plots for the Vir, Regeneron, AstraZeneca, Lilly and Adagio antibodies.

Figure 3. Interaction of B.1.617.1 and B.1.617.2 with ACE2. (A) BLI experiments showing the binding of ACE2 to RBDs of B.1.617.1, B.1.617.2 and the T478K mutant. Experimental data for the dilution series are shown in different colors and the models as red lines. (B) Neutralisation data (NT50) and BLI data (K_D) mapped onto the RBD using the

method described (Dejnirattisai *et al.*, 2021). The top two panels show the NT50 and K_D values respectively for B.1.617.1 whilst the lower two panels show the corresponding values for B.1.617.2. Front and back views of the RBD are shown. the spheres represent the antibody binding sites coloured according to the ratio of the values for B.1.617.1/Wuhan and B.1.617.2/Wuhan. The NT50 plots are coloured according to white for a ratio of 1, for red it is <0.001 (i.e. at least 1000-fold reduction), blue indicates that the binding is increased). For the K_D plots white denotes a ratio of 1, for red it is <0.1 (i.e. at least 10-fold reduction), black dots refer to mapped antibodies not included in this analysis, dark green RBD ACE2 binding surface, blue show the mutated residues in each variant. Note the strong agreement between NT50 and $K_{D.}$ All relevant data are shown in **Table S1**. (C) K_D of RBD/mAb interaction measured by BLI for RBDs of Victoria, B.1.1.7, P.1 and B.1.351 (left to right).

Figure 4. Crystals structures of RBD-Fab complexes and mechanism of reduced antibody potency to B.1.617 variants. (A) Cartoon depiction of the ternary complex of Wuhan RBD (grey, magenta balls represent the mutations in the B.1.617 lineage and this representation is also used on other panels) with antibody 278 (light chain blue, heavy chain red) and antibody 222 (light chain pale blue, heavy chain pink) which was used as a crystallization chaperone. The heavy chain of antibody 278 binds to an epitope comprising residue 452 explaining its reduced ability to neutralize both B.1.617.1 and B.1.617.2. (B) Simplification of (A) showing CDR loop H3 from antibody 278 (HC red, LC blue) interacting with residue 452 on the Wuhan RBD depicted as a grey surface (again the B.1.617 lineage mutations are highlighted in magenta). (C), (D) Specifics of antibody 278 interaction. (C) Residue D108 of H3 forms salt bridges with R346, K444 and N450. L452R would sterically inhibit binding. (D) L1 salt-bridges via S31 to R346 of the RBD, Y32 hydrogen bonds to the carbonyl of D442. L3 forms backbone hydrogen bond interactions

between Y92 and K444, T94 and G446. (E), (F) The binding mode of Fab 384 (E) and its interactions with L452 and E484 of the RBD (F) (PDB ID 7BEP). (G) Cartoon depiction of the ternary complex of antibody 253 (HC red (sugar in red sticks), LC blue) with mutant L452R RBD (grey with sugar shown as sticks) with antibody 75 (HC pink, LC green) used as a crystallization chaperone. Antibody 253 makes no contact with R452 in line with no observed loss of neutralization (H) Cartoon depiction of ternary complex of antibody 253 (HC red, LC blue, sugar red sticks) with T478K RBD (grey) and antibody 45 (HC pink, LC green) as a crystallization chaperone. (I, J) Close-ups showing 253 interacting with residue 478 in the two mutant RBDS revealing a modest shift in the binding pose of 253. The L452R mutant RBD is in dark grey with antibody 253 in crimson (HC) and blue (LC) whilst the T478K RBD is in white with 253 in pink (HC) and pale blue (LC). The Thr and Lysine at 478 are shown as magenta sticks (I). In the T478K mutant RBD, the lysine folds back away from the antibody (J). (K), (L) The binding mode of Fab 316 to RBD (K) and its interactions with E484 of the RBD (L) (PDB ID 7BEH).

Figure 5. Neutralization of B.1.617.1 by convalescent serum. (A) Neutralization of three (A, B, C) B.1.617.1 pseudotyped lentiviruses, by convalescent plasma (n=34) collected from volunteers 4-9 weeks following SARS-CoV-2 infection, all samples were collected before June 2020 and therefore represent infection before the emergence of B.1.1.7 in the UK. Comparison is made with neutralization curves for pseudovirus Victoria. (B) Comparison of FRNT50 titres for B.1.617-A, B.1.617-B, B.1.617-C with Victoria, geometric mean titres are shown above each column. Neutralization titres for Victoria and B.1.617-B pseudovirus using (C) B.1.1.7 convalescent serum, (D) B.1.351 convalescent serum and (C) P.1 convalescent serum. The Wilcoxon matched-pairs signed rank test was used for the analysis

and two-tailed P values were calculated. For the data presented for B.1.1.7 in (B) the sample with extremely high titres was excluded from the statistical analysis.

Figure 6 Neutralization of B.1.617.2 by convalescent plasma. (A) Neutralization of B.1.617.2 live virus measured by FRNT using the 34 convalescent samples described in **Figure 5A**, comparison is made with neutralization titres to Victoria, B.1.1.7, B.1.351 and P.1 (filled squares) previously reported in (Supasa et al., 2021; Zhou et al., 2021; Dejnirattisai et al., 2021b), geometric mean titres are shown above each column. Neutralization titres for Victoria, B.1.1.7, B.1.351, P.1 and B.1.617.2 using (B) B.1.1.7 convalescent plasma, (C) B.1.351 convalescent serum and (D) P.1 convalescent serum. The green arrow in (C) represents serum from an individual who was infected with B.1.351 and subsequently received a vaccine. The Wilcoxon matched-pairs signed rank test was used for the analysis and two-tailed P values were calculated. For the data presented for B.1.1.7 in (B) the sample with extremely high titres was excluded from the statistical analysis. Neutralization curves for Victoria, B.1.1.7, B.1.351, P.1 and B.1.617.2 using convalescent serum from (E) B.1.351 and (F) P.1 infected individuals.

Figure 7 Neutralization by vaccine serum and mapping variants in antigenic space. Pfizer vaccine, serum (n=25) was taken 7-17 days following the second dose of the Pfizer-BioNTech vaccine. AstraZenca vaccine, serum was taken 14 or 28 days following the second dose of the Oxford-AstraZeneca vaccine (n=25). (A) NT50 titres of Pfizer-BioNTech serum against B.1.617.1-B pseudo virus. (B) FRNT50 titres of Oxford-AstraZeneca serum against B.1.617.1-B pseudovirus. (C) FRNT50 titres of Pfizer-BioNTech serum against B.1.617.2 virus. (D) FRNT50 against of Oxford-AstraZeneca serum against B.1.617.2 virus. Comparison is made with Victoria pseudo virus (A,B) or wild type Victoria, B.1.1.7,

B.1.351 and P.1 (filled squares) previously reported in (Supasa et al., 2021; Zhou et al., 2021; Dejnirattisai et al., 2021b) (C, D). Subsequent panels analyze responses following a single dose of Pfizer vaccine. Serum (n=20) was taken 28 or 70 days following the first dose of the Pfizer-BioNTech vaccine. (E, F) Comparison of FRNT50 titres for individual samples obtained 28 or 70 days after the first dose against Victoria or B.1.617.2. (G and H) Comparison of percent virus neutralization at serum dilution 1:20 against SARS-CoV-2 Victoria and B.1.617.2 strains. Mean values are indicated above each column. The Mann-Whitney unpaired test was used for the analysis E, G. The Wilcoxon matched-pairs signed rank test was used for the analysis F, H. (I) Map of variants in antigenic space. Wall-eyed stereo pair plots showing output of principle component analysis converting serum/virus strain pair neutralisation capacities to antigenic space. Circle size denotes depth along axis connecting the reader's nose to the origin. See also Video S1. (J) Positions and charge effects of RBD mutations found in variants of concern. Incoming ACE2 view of the surface of the RBD with the footprint of ACE2 shown in green and mutations occurring in variants including B.1.1.7, P.1, P.1.351, B.1.617.1 and B.1.617.2, are shown in a range of other colours.

STAR Methods

RESOURCE AVAILABILITY

Lead Contact

Resources, reagents and further information requirement should be forwarded to and will be responded by the Lead Contact, David I Stuart (dave@strubi.ox.ac.uk).

Materials Availability

Reagents generated in this study are available from the Lead Contact with a completed Materials Transfer Agreement.

Data and Code Availability

The coordinates and structure factors of the crystallographic complexes are available from the PDB with accession codes: 7OR9, 7ORA, 7ORB (see **Table S1**). Mabscape is available from https://github.com/helenginn/mabscape, https://snapcraft.io/mabscape. The data that support the findings of this study are available from the corresponding authors on request.

EXPERIMENTAL MODEL AND SUBJECT DETAILS

Viral stocks

SARS-CoV-2/human/AUS/VIC01/2020 (Caly et al., 2020), SARS-CoV-2/B.1.1.7 and SARS-CoV-2/B.1.351 were provided by Public Health England, P.1 from a throat swab from Brazil were grown in Vero (ATCC CCL-81) cells. Cells were infected with the SARS-CoV-2 virus using an MOI of 0.0001. Virus containing supernatant was harvested at 80% CPE and spun at 3000 rpm at 4 °C before storage at -80 °C. Viral titres were determined by a focus-forming assay on Vero cells. Victoria passage 5, B.1.1.7 passage 2 and B.1.351 passage 4 stocks P.1 passage 1 stocks were sequenced to verify that they contained the expected spike protein sequence and no changes to the furin cleavage sites. The B.1.617.2 virus was kindly provided Wendy Barclay and Thushan De Silva contained the following mutations compared to the Wuhan sequence T19R, G142D, Δ156-157/R158G, A222V, L452R, T478K, D614G, P681R, D950N.

Bacterial Strains and Cell Culture

Vero (ATCC CCL-81) cells were cultured at 37 °C in Dulbecco's Modified Eagle medium (DMEM) high glucose (Sigma-Aldrich) supplemented with 10% fetal bovine serum (FBS), 2 mM GlutaMAX (Gibco, 35050061) and 100 U/ml of penicillin–streptomycin. Human mAbs

were expressed in HEK293T cells cultured in UltraDOMA PF Protein-free Medium (Cat# 12-727F, LONZA) at 37 °C with 5% CO_2. *E.coli DH5α* bacteria were used for transformation of plasmids encoding wt and mutated RBD proteins. A single colony was picked and cultured in LB broth with 50 µg mL^{-1} Kanamycin at 37 °C at 200 rpm in a shaker overnight. HEK293T (ATCC CRL-11268) cells were cultured in DMEM high glucose (Sigma-Aldrich) supplemented with 10% FBS, 1% 100X Mem Neaa (Gibco) and 1% 100X L-Glutamine (Gibco) at 37 °C with 5% CO_2. To express RBD, RBD variants and ACE2, HEK293T cells were cultured in DMEM high glucose (Sigma) supplemented with 2% FBS, 1% 100X Mem Neaa and 1% 100X L-Glutamine at 37 °C for transfection.

Plasma from early pandemic and B.1.1.7 cases

Participants from the first wave of SARS-CoV2 in the U.K. and those sequence confirmed with B.1.1.7 lineage in December 2020 and February 2021 were recruited through three studies: Sepsis Immunomics [Oxford REC C, reference:19/SC/0296]), ISARIC/WHO Clinical Characterisation Protocol for Severe Emerging Infections [Oxford REC C, reference 13/SC/0149] and the Gastro-intestinal illness in Oxford: COVID sub study [Sheffield REC, reference: 16/YH/0247]. Diagnosis was confirmed through reporting of symptoms consistent with COVID-19 and a test positive for SARS-CoV-2 using reverse transcriptase polymerase chain reaction (RT-PCR) from an upper respiratory tract (nose/throat) swab tested in accredited laboratories. A blood sample was taken following consent at least 14 days after symptom onset. Clinical information including severity of disease (mild, severe or critical infection according to recommendations from the World Health Organisation) and times between symptom onset and sampling and age of participant was captured for all individuals at the time of sampling. Following heat inactivation of plasma/serum samples they were aliquoted so that no more than 3 freeze thaw cycles were performed for data generation.

Sera from B.1.351 and P.1infected cases

B.1.351 samples from UK infected cases was collected under the "Innate and adaptive immunity against SARS-CoV-2 in healthcare worker family and household members" protocol affiliated to the Gastro-intestinal illness in Oxford: COVID sub study discussed above and approved by the University of Oxford Central University Research Ethics Committee. All individuals had sequence confirmed B.1.351 infection or PCR-confirmed symptomatic disease occurring whilst in isolation and in direct contact with B.1.351 sequence-confirmed cases. Additional B.1.351 infected serum (sequence confirmed) was obtained from South Africa. At the time of swab collection patients signed an informed consent to consent for the collection of data and serial blood samples. The study was approved by the Human Research Ethics Committee of the University of the Witwatersrand (reference number 200313) and conducted in accordance with Good Clinical Practice guidelines. P.1 samples were provided by the International Reference Laboratory for Coronavirus at FIOCRUZ (WHO) as part of the national surveillance for coronavirus and had the approval of the FIOCRUZ ethical committee (CEP 4.128.241) to continuously receive and analyse samples of COVID-19 suspected cases for virological surveillance. Clinical samples were shared with Oxford University, UK under the MTA IOC FIOCRUZ 21-02.

Sera from Pfizer vaccinees

Pfizer vaccine serum was obtained from volunteers who had received either one or two doses of the BNT162b2 vaccine. Vaccinees were Health Care Workers, based at Oxford University Hospitals NHS Foundation Trust, not known to have prior infection with SARS-CoV-2 and were enrolled in the OPTIC Study as part of the Oxford Translational Gastrointestinal Unit GI Biobank Study 16/YH/0247 [research ethics committee (REC) at Yorkshire & The Humber – Sheffield]. The study was conducted according to the principles of the Declaration of Helsinki

(2008) and the International Conference on Harmonization (ICH) Good Clinical Practice (GCP) guidelines. Written informed consent was obtained for all participants enrolled in the study. Two groups were studied after receiving COVID-19 mRNA Vaccine BNT162b2, 30 micrograms, administered intramuscularly after dilution (0.3 mL each). A "short dosing interval" group were sampled 7-17 days after receiving two doses of vaccine 18-28 days apart, and a "long dosing interval" group were sampled twice, approximately 28 days (range 25-35) and 70 days (range 48-93) after receiving a single dose of the vaccine. The mean age of vaccines was 37 years (range 22-66), 21 male and 35 female.

AstraZeneca-Oxford vaccine study procedures and sample processing

Full details of the randomized controlled trial of ChAdOx1 nCoV-19 (AZD1222), were previously published (PMID: 33220855/PMID: 32702298). These studies were registered at ISRCTN (15281137 and 89951424) and ClinicalTrials.gov (NCT04324606 and NCT04400838). Written informed consent was obtained from all participants, and the trial is being done in accordance with the principles of the Declaration of Helsinki and Good Clinical Practice. The studies were sponsored by the University of Oxford (Oxford, UK) and approval obtained from a national ethics committee (South Central Berkshire Research Ethics Committee, reference 20/SC/0145 and 20/SC/0179) and a regulatory agency in the United Kingdom (the Medicines and Healthcare Products Regulatory Agency). An independent DSMB reviewed all interim safety reports. A copy of the protocols was included in previous publications (PMID: 33220855/PMID: 32702298).

Data from vaccinated volunteers who received two vaccinations are included in this paper. Vaccine doses were either 5×10^{10} viral particles (standard dose; SD/SD cohort n=21) or half dose as their first dose (low dose) and a standard dose as their second dose (LD/SD cohort

n=4). The interval between first and second dose was in the range of 8-14 weeks. Blood samples were collected and serum separated on the day of vaccination and on pre-specified days after vaccination e.g. 14 and 28 days after boost.

METHOD DETAILS

Focus Reduction Neutralization Assay (FRNT)

The neutralization potential of Ab was measured using a Focus Reduction Neutralization Test (FRNT), where the reduction in the number of the infected foci is compared to a negative control well without antibody. Briefly, serially diluted Ab or plasma was mixed with SARS-CoV-2 strain Victoria or P.1 and incubated for 1 hr at 37 °C. The mixtures were then transferred to 96-well**,** cell culture-treated, flat-bottom microplates containing confluent Vero cell monolayers in duplicate and incubated for a further 2 hrs followed by the addition of 1.5% semi-solid carboxymethyl cellulose (CMC) overlay medium to each well to limit virus diffusion. A focus forming assay was then performed by staining Vero cells with human anti-NP mAb (mAb206) followed by peroxidase-conjugated goat anti-human IgG (A0170; Sigma). Finally, the foci (infected cells) approximately 100 per well in the absence of antibodies, were visualized by adding TrueBlue Peroxidase Substrate. Virus-infected cell foci were counted on the classic AID EliSpot reader using AID ELISpot software. The percentage of focus reduction was calculated and IC_{50} was determined using the probit program from the SPSS package.

Plasmid construction and pseudotyped lentiviral particles production

The constructs of pseudotyped lentivirus expressing SARS-CoV-2 S proteins are as previously described in Nie et al. (Nie et al., 2020), with some modifications. Briefly, the

gene sequences were designed to encode S protein of Victoria (S247R), B.1.617.1A (E154K, L452R, E484Q, D614G, P681R, E1072K and K1073R), B.1.617.1B (T95I, G142D, E154K, L452R, E484Q, D614G, P681R and Q1071H), B.1.617.1C (L452R, E484Q, D614G and P681R), B.1.617.2 (T19R, 156-158del, L452R, T478K, D614G, P681R and D950N), B.1.1.519 (T478K, D614G, P681H and T732A) or B.1.429 (S13I, W152C, L452R and D614G). A synthetic codon-optimised SARS-CoV-2 construct from Wuhan-Hu-1 (GenBank: MN908947) was used as the template and the constructs were cloned by PCR amplification of vector and inserts, followed by Gibson assembly. To generate the insert fragments, the overlapping primers for all individual variants were used separately to amplify, together with two primers of pcDNA3.1 vector (pcDNA3.1_BamHI_F and pcDNA3.1_Tag_S_EcoRI_R). The pcDNA3.1 vector was also amplified using pcDNA3.1_Tag_S_EcoRI_F and pcDNA3.1_BamHI_R primers. The primer pairs used in this study are shown in supplementary (**Table S5**). All constructs were verified by Sanger sequencing.

Production of pseudotyped lentiviral particles expressing SARS-CoV-2 S protein was carried out as described previously (di Genova et al., 2020), with some modifications. Briefly, HEK293T/17 cells (ATCC® CRL-11268™) were co-transfected with three essential plasmids; plasmid (pCDNA 3.1) expressing SARS-CoV-2 S protein (Victoria or B.1.617.1 or B.1.1.519), lentiviral vector expressing firefly luciferase reporter protein (pCSFLW), and the second generation of lentiviral packaging plasmid (p8.91) expressing gag, pol and rev proteins at the ratio of 1:1.5:1 µg, respectively, in 200 µl opti-MEM (Gibco). The DNA cocktails were then supplemented with the equal volume of opti-MEM containing 35 µL of 1 mg/mL polyethylenimine (Sigma-Aldrich). After 20 min incubation, the plasmid DNA-PEI complexes were then added into the T75 cm^2 culture flask containing approximate 50% confluency of HEK293T/17 cells. The medium was changed twice, one hour prior to

transfection and 18-24 h post transfection. The culture supernatant containing pseudotyped lentiviral particles were harvested at 72 h post-transfection by centrifugation and kept at -80 °C. In each experiment, 90 ng/mL of HIV- gag protein was normalized using the RETROtek HIV-1 p24 Antigen-ELISA kit (Zeptometrix; Buffalo, NY), according to manufacturer's instructions.

A similar strategy was used to produce lentiviral vector carrying human ACE2 (hACE2). However, the plasmid expressing SARS-CoV-2 S and luciferase reporter proteins were replaced by the Vesicular stomatitis virus G protein (pCMV-VSV-G) and vector expressing human ACE2 (pHR-SIN-ACE2). Both plasmids were kindly provided by Alain Townsend. The resulting lentiviral particles were transduced into HEK293T/17 cells to generate the stable expressing hACE2 receptor. The transduced cells were subjected to hACE2 staining and single cell sorting, clones with >80% hACE2 positive cells were used as the target cells for pseudotyped based neutralization assays.

Pseudoviral neutralization assay

Pseudotyped lentiviral particles expressing SARS-CoV2 S protein (Victoria or B.1.617 or B.1.1.519) were incubated with serial dilutions of mAbs or plasma in white opaque 96-well plates at 37˚C, 5% CO2 for 1 hr. The stable HEK293T/17 cells expressing human ACE2 were then added to the mixture at $1.5x10^4$ cells/well. Plates were spun at 500 RCF for 1 min and further incubated for another 48 hr. Culture supernatants were removed and 50 µL of 1:2 Bright-GloTM Luciferase assay system (Promega, USA) in 1X PBS (sigma) was added to each well. The reaction was incubated at room temperature for 5 mins and the firefly luciferase activity was measured using CLARIOstar® (BMG Labtech). The percentage of

neutralization of mAbs or plasma samples towards pseudotyped lentiviruses was calculated relative to the control.

Cloning of ACE2 and RBD proteins

The constructs of ACE2, WT RBD, B.1.1.7, B.1.351 and P.1 mutant RBD are the same as previously described (Dejnirattisai et al. 2021, Zhou et al., 2021, Supasa et al., 2021). To clone RBD expression plasmids which has the same nucleotide optimization with the spike of pseudovirus (RBD-PV), the sRBD fragment were amplified from pcDNA 3.1- SARS-CoV-2 Spike plasmids using primers of PV-RBD. pNEO vector was digested by AgeI and KpnI and joined with RBD fragments by Gibson assembly.

To construct RBD L452R and T478K, primers of L452R and primers of T478K were used separately, together with two primers of pNEO vector to do PCR, with the plasmid of RBD-PV as the template. To construct RBD L452R T478K and RBD L452R E484Q, primers of T478K and RBD E484Q were used to pair with the primers of pNEO vector to do PCR, with the plasmid of RBD L452R as template. Two PCR fragments amplified for each mutation were purified by QIAquick Gel Extraction Kit (Qiagen, Hilden, Germany) and used as templates to be joined together by further PCR with the two primers of pNEO vector. Amplified DNA fragments were digested with restriction enzymes AgeI and KpnI and then ligated into digested pNEO vector. All constructs were verified by sequencing.

Protein production

Protein production was as described in Zhou et al. (Zhou et al., 2020). Briefly, plasmids encoding proteins were transiently expressed in HEK293T (ATCC CRL-11268) cells. The conditioned medium was dialysed and purified with a 5-ml HisTrap nickel column (GE

Healthcare) and further polished using a Superdex 75 HiLoad 16/60 gel filtration column (GE Healthcare).

Bio-Layer Interferometry

BLI experiments were run on an Octet Red 96e machine (Fortebio). To measure the binding affinity of ACE2 with different RBD variants, each RBD was immobilized onto AR2G biosensors (Fortebio) and serial dilutions of ACE2 were used as analytes. To measure the binding affinity of monoclonal antibodies with RBD variants, each his-tagged RBD was immobilized onto Ni-NTA biosensors (Fortebio) and antibodies (Dejnirattisai et al., 2021a) were used as analytes All experiments were run at 30 °C. Data were recorded using software Data Acquisition 11.1 (Fortebio) and Data Analysis HT 11.1 (Fortebio) with a 1:1 fitting model used for the analysis.

Antibody production

AstraZeneca and Regeneron antibodies were provided by AstraZeneca, Vir, Lilly and Adagio antibodies were provided by Adagio. For the antibodies heavy and light chains of the indicated antibodies were transiently transfected into 293Y cells and antibody purified from supernatant on protein A.

Crystallization

WT RBD was mixed with 222 Fab and 278 Fab, L452R mutant RBD was mixed with 75 Fab and 253 Fab, and T478K mutant RBD was mixed with 45 Fab and 253 Fab in a 1:1:1 molar ratio to a final concentration of 7.0 mg ml^{-1}. All samples were incubated at room temperature for 30 min. Crystallization experiments were set up with a Cartesian Robot in Crystalquick 96-well X plates (Greiner Bio-One) using the nanoliter sitting-drop vapor-diffusion method,

with 100 nl of protein plus 100 nl of reservoir in each drop, as previously described (Walter et al., 2003). Good crystals of WT RBD/222-278 Fab complex were obtained from Molecular Dimensions Morpheus condition H1, containing 0.1 M amino acids (Glu, Ala, Gly, Lys, Ser), 0.1 M MES/imidazole pH 6.5, 10% (w/v) PEG 20000 and 20% (v/v) PEG MME 550. Good crystals of L452R mutant RBD/75-253 complex were obtained from Hampton Research PEGRx condition 44, containing 0.1 M BIS-TRIS pH 6.5 and 16% (w/v) PEG 10000. Crystals of T478K mutant RBD/45-253 complex were obtained from Hampton Research PEGRx condition 45, containing 0.1 M BICINE pH 8.5 and 20% (w/v) PEG 10,000.

X-ray data collection, structure determination and refinement

Crystals of WT RBD/222-278 Fab complex were mounted in loops and frozen by directly dipping in liquid nitrogen. Crystals of L452R mutant RBD/75-253 and T478K mutant RBD/45-253 complexes were mounted and dipped in solution containing 25% glycerol and 75% mother liquor for a second before being frozen in liquid nitrogen. Diffraction data were collected at 100 K at beamline I03 of Diamond Light Source, UK. All data were collected as part of an automated queue system allowing unattended automated data collection (https://www.diamond.ac.uk/Instruments/Mx/I03/I03-Manual/Unattended-Data-Collections.html). Diffraction images of 0.1° rotation were recorded on an Eiger2 XE 16M detector (exposure time of either 0.006 or 0.009 s per image, beam size 80×20 μm, 100% beam transmission and wavelength of 0.9763 Å). Data were indexed, integrated and scaled with the automated data processing program Xia2-dials (Winter, 2010;Winter *et al.*, 2018). Data of 360° was collected from a frozen crystal for each of the WT RBD/222-278 and T478K-RBD/45-253 Fab complexes. Data set of L452R-RBD/75-253 were merged from four crystals (360° from each crystal).

Structures were determined by molecular replacement with PHASER (McCoy et al., 2007) using search models of SARS-CoV-2 RBD-EY6A-222 (PDB ID 7NX6) (Dejnirattisai et al., 2021b) for RBD/222-278 complex, RBD/75-253 (PDB ID, 7BEN) (Dejnirattisai et al., 2021a) for L452R-RBD/75-253 complex, and RBD/45-88 (PDB ID, 7BEL) and RBD/75-253 (PDB ID, 7BEN) (Dejnirattisai et al., 2021a). Model rebuilding with COOT (Emsley and Cowtan, 2004) and refinement with PHENIX (Liebschner et al., 2019) were done for all the structures. There is one ternary complex in the asymmetric unit of RBD/222-278 crystal, and two complexes in the asymmetric unit of both L452R-RBD/75-253 and T478K-RBD/45-253 crystals. The ChCl domains of Fab 45 in the T478K-RBD/45-253 complex are flexible and have poor electron density. Data collection and structure refinement statistics are given in **Table S2**. Structural comparisons used SHP (Stuart et al., 1979), residues forming the RBD/Fab interface were identified with PISA (Krissinel and Henrick, 2007) and figures were prepared with PyMOL (The PyMOL Molecular Graphics System, Version 1.2r3pre, Schrödinger, LLC).

Antigenic Space Plots

Log of IC_{50} values for each serum/virus strain pair were assembled into vectors for each virus strain. 113 sera from a range of natural infections and vaccinations were used in total and compared against 7 virus strains, assembling a 113x7 matrix. Single value decomposition of this serum/virus strain pair matrix was carried out, producing weighted orthogonal vectors representing the axes of variation within the data and each strain was expressed as a vector in this new orthogonal basis. The largest axis of variation was largely identical for each strain, representing the positivity in common with all log dilution values. The 2nd, 3rd and 4th major axes were plotted using cluster4x (Ginn, 2020) to show the separation between each virus strain in antigenic space.

Quantification and statistical analysis

Statistical analyses are reported in the results and figure legends. Neutralization was measured by FRNT. The percentage of focus reduction was calculated and IC_{50} was determined using the probit program from the SPSS package. The Wilcoxon matched-pairs signed rank test was used for the analysis and two-tailed P values were calculated and geometric mean values. BLI data were analysed using Data Analysis HT 11.1 (Fortebio) with a 1:1 fitting model.

Supplementary Figures

Figure S1. Neutralization curves of twenty human monoclonal antibodies against SARS-CoV-2 pseudo typed lentiviruses expressing full-length spike of B.1.617.1, B.1.617.2, B.1.1.519 and B.1.429 variants, related to Figure 2. FRNT50 titers are given in Table S2.

Figure S2. Structure features of SARS-CoV-2 mAbs and effects of B.1.617 mutations. (A) In the left panel, comparing the binding modes of fab 278 (red and blue) and Fab 75 (salmon and teal), and the right panel showing the CDR loops of the two Fabs involved in contacts with the RBD. The mutation sites, L452, T478 and E484, of B.1.617 variants are highlighted in magenta. (B) The left panel comparing the binding mode of fab 278 (red and blue) with that of REGN-10987 (salmon and teal, PDB ID 6XDG), and the right panel showing the CDR loops of the two Fabs involved in contacts with the RBD. (C) Electron density maps contoured at 1.0 σ showing the density for R452 in the L452R-RBD/75-253 complex (left), and K478 in the T478K-RBD/45-253 complex. (D), (E) Positions of the mutation sites in the NTD of the B.1.617.1 (D) and B.1.617.2 (E) spike relative to the bound antibody 159 (PDB ID 7NDC). The VhVl domains of mAb 159 are shown as surfaces and the NTD as grey

ribbons with mutation and deletion sites marked with green and magenta spheres, respectively. Related to Figure 4.

Figure S3. Neutralization curves against SARS-CoV-2 pseudo typed lentiviruses expressing full-length spike of Victoria and B.1.617.1 strains by (A) plasma from 18 patients infected with B.1.1.7 (B) serum from 14 patients infected with B.1.351 (C) serum from 17 patients infected with P.1, related to Figure 5. FRNT50 titers are given in Table S3.

Figure S4. Neutralization curves against authentic SARS-CoV-2-Victoria, B.1.1.7, B.1.351, P.1 and B.1.617.2 strains by (A) plasma from 34 patients during early pandemic UK (B) serum from 14 patients infected with B.1.1.7, related to Figure 6. FRNT50 titers given in Table S3.

Figure S5. Neutralization curves against SARS-CoV-2 pseudo typed lentiviruses expressing full-length spike of Victoria and B.1.617.1 strains by (A) Serum from 25 recipients of Pfizer-BioNTech vaccine. (B) Oxford-AstraZeneca vaccine, related to Figure 7. FRNT50 titers given in Table S4.

Figure S6. Neutralization curves against authentic SARS-CoV-2-Victoria, B.1.1.7, B.1.351, P.1 and B.1.617.2 strains by (A) Serum from 25 recipients of Pfizer-BioNTech vaccine. (B) Oxford-AstraZeneca vaccine, related to Figure 7. FRNT50 titers given in Table S4.

Video S1. 3D view of antigenic space plot for current variants, related to Fig. 7I.

References

COG-UK Consortium (2020). An integrated national scale SARS-CoV-2 genomic surveillance network. The Lancet Microbe 1, e99–e100.

Baden, L.R., El Sahly, H.M., Essink, B., Kotloff, K., Frey, S., Novak, R., Diemert, D., Spector, S.A., Rouphael, N., Creech, C.B., et al. (2020). Efficacy and Safety of the mRNA-1273 SARS-CoV-2 Vaccine. N. Engl. J. Med. 384, 403-416.

Baum, A., Fulton, B.O., Wloga, E., Copin, R., Pascal, K.E., Russo, V., Giordano, S., Lanza, K., Negron, N., Ni, M., et al. (2020). Antibody cocktail to SARS-CoV-2 spike protein prevents rapid mutational escape seen with individual antibodies. Science *369,* 1014–1018.

Caly, L., Druce, J., Roberts, J., Bond, K., Tran, T., Kostecki, R., Yoga, Y., Naughton, W., Taiaroa, G., Seemann, T., et al. (2020). Isolation and rapid sharing of the 2019 novel coronavirus (SARS-CoV-2) from the first patient diagnosed with COVID-19 in Australia. Med. J. Aust. 212, 459–462.

Cerutti, G., Guo, Y., Zhou, T., Gorman, J., Lee, M., Rapp, M., Reddem, E.R., Yu, J., Bahna, F., Bimela, J., et al. (2021). Potent SARS-CoV-2 neutralizing antibodies directed against spike N-terminal domain target a single supersite. Cell Host Microbe 29, 819-833.

Chi, X., Yan, R., Zhang, J., Zhang, G., Zhang, Y., Hao, M., Zhang, Z., Fan, P., Dong, Y., Yang, Y., et al. (2020). A neutralizing human antibody binds to the N-terminal domain of the Spike protein of SARS-CoV-2. Science 369, 650–655.

Dejnirattisai, W., Zhou, D., Ginn, H.M., Duyvesteyn, H.M.E., Supasa, P., Case, J.B., Zhao, Y., Walter, T.S., Mentzer, A.J., Liu, C., et al. (2021a). The antigenic anatomy of SARS-CoV-2 receptor binding domain. Cell https://doi.org/10.1016/j.cell.2021.02.032.

Dejnirattisai, W., Zhou, D., Supasa, P., Liu, C., Mentzer, A.J., Ginn, H.M., Zhao, Y., Duyvesteyn, H.M.E., Tuekprakhon, A., Nutalai, R., et al. (2021b). Antibody evasion by the Brazilian P.1 strain of SARS-CoV-2. BioRxiv https://doi.org/10.1101/2021.03.12.435194.

Deng, X., Garcia-Knight, M.A., Khalid, M.M., Servellita, V., Wang, C., Morris, M.K., Sotomayor-González, A., Glasner, D.R., Reyes, K.R., Gliwa, A.S., et al. (2021). Transmission, infectivity, and neutralization of a spike L452R SARS-CoV-2 variant. Cell 184, 1-12.

Domingo, E., Sheldon, J., and Perales, C. (2012). Viral Quasispecies Evolution. Microbiol. Mol. Biol. Rev. 76, 159–216.

Emary, K.R.W., Golubchik, T., Aley, P.K., Ariani, C. V., Angus, B., Bibi, S., Blane, B., Bonsall, D., Cicconi, P., Charlton, S., et al. (2021). Efficacy of ChAdOx1 nCoV-19 (AZD1222) vaccine against SARS-CoV-2 variant of concern 202012/01 (B.1.1.7): an exploratory analysis of a randomised controlled trial. Lancet 397, 1351–1362.

Emsley, P., and Cowtan, K. (2004). Coot: Model-building tools for molecular graphics. Acta Crystallogr. Sect. D Biol. Crystallogr. 60, 2126–2132.

Folegatti, P.M., Ewer, K.J., Aley, P.K., Angus, B., Becker, S., Belij-Rammerstorfer, S., Bellamy, D., Bibi, S., Bittaye, M., Clutterbuck, E.A., et al. (2020). Safety and immunogenicity of the ChAdOx1 nCoV-19 vaccine against SARS-CoV-2: a preliminary report of a phase 1/2, single-blind, randomised controlled trial. Lancet 396, 467–478.

Fonville, J.M., Wilks, S.H., James, S.L., Fox, A., Ventresca, M., Aban, M., Xue, L., Jones, T.C., Le, N.M.H., Pham, Q.T., et al. (2014). Antibody landscapes after influenza virus infection or vaccination. Science 346, 996–1000.

di Genova, C., Sampson, A., Scott, S., Cantoni, D., Mayora-Neto, M., Bentley, E., Mattiuzzo, G., Wright, E., Derveni, M., Auld, B., et al. (2020). Production, titration, neutralisation and storage of SARS-CoV-2 lentiviral pseudotypes. [online] Available at: <https://figshare.com/articles/preprint/Production_titration_neutralisation_and_storage_of_SARS-CoV-2_lentiviral_pseudotypes/13502580/2> [Accessed 20 May 2021].

Ginn, H.M. (2020). Pre-clustering data sets using cluster 4 x improves the signal-to-noise ratio of high-throughput crystallography drug-screening analysis. Acta Crystallogr. Sect. D Struct. Biol. 76, 1134–1144.

Gorbalenya, A.E., Baker, S.C., Baric, R.S., de Groot, R.J., Drosten, C., Gulyaeva, A.A., Haagmans, B.L., Lauber, C., Leontovich, A.M., Neuman, B.W., et al. (2020). The species Severe acute respiratory syndrome-related coronavirus: classifying 2019-nCoV and naming it SARS-CoV-2. Nat. Microbiol. 5, 536–544.

Greaney, A.J., Starr, T.N., Gilchuk, P., Zost, S.J., Binshtein, E., Loes, A.N., Hilton, S.K., Huddleston, J., Eguia, R., Crawford, K.H.D., et al. (2021). Complete Mapping of Mutations to the SARS-CoV-2 Spike Receptor-Binding Domain that Escape Antibody Recognition. Cell Host Microbe 29, 44-57.e9.

Hoffmann, M., Kleine-Weber, H., Schroeder, S., Mü, M.A., Drosten, C., and Pö, S. (2020). SARS-CoV-2 Cell Entry Depends on ACE2 and TMPRSS2 and Is Blocked by a Clinically Proven Protease Inhibitor. Cell 181, 271-280.e8.

Kemp, S.A., Collier, D.A., Datir, R.P., Ferreira, I.A.T.M., Gayed, S., Jahun, A., Hosmillo, M., Rees-Spear, C., Mlcochova, P., Lumb, I.U., et al. (2021). SARS-CoV-2 evolution during treatment of chronic infection. Nature https://doi.org/10.1038/s41586-021-03291-y.

Krammer, F. (2020). SARS-CoV-2 vaccines in development. Nature 586, 516–527.

Kreye, J., Reincke, S.M., Kornau, H.C., Sánchez-Sendin, E., Corman, V.M., Liu, H., Yuan, M., Wu, N.C., Zhu, X., Lee, C.C.D., et al. (2020). A Therapeutic Non-self-reactive SARS-CoV-2 Antibody Protects from Lung Pathology in a COVID-19 Hamster Model. Cell 183, 1058–1069.

Krissinel, E., and Henrick, K. (2007). Inference of Macromolecular Assemblies from Crystalline State. J. Mol. Biol. 372, 774–797.

Ku, Z., Xie, X., Davidson, E., Ye, X., Su, H., Menachery, V.D., Li, Y., Yuan, Z., Zhang, X., Muruato, A.E., et al. (2021). Molecular determinants and mechanism for antibody cocktail preventing SARS-CoV-2 escape. Nat. Commun. 12, 469.

Lan, J., Ge, J., Yu, J., Shan, S., Zhou, H., Fan, S., Zhang, Q., Shi, X., Wang, Q., Zhang, L., et al. (2020). Structure of the SARS-CoV-2 spike receptor-binding domain bound to the ACE2 receptor. Nature 581, 215–220.

Liebschner, D., Afonine, P. V., Baker, M.L., Bunkoczi, G., Chen, V.B., Croll, T.I., Hintze, B., Hung, L.W., Jain, S., McCoy, A.J., et al. (2019). Macromolecular structure determination using X-rays, neutrons and electrons: Recent developments in Phenix. Acta Crystallogr. Sect. D Struct. Biol. 75, 861–877.

Lu, R., Zhao, X., Li, J., Niu, P., Yang, B., Wu, H., Wang, W., Song, H., Huang, B., Zhu, N., et al. (2020). Genomic characterisation and epidemiology of 2019 novel coronavirus: implications for virus origins and receptor binding. Lancet 395, 565–574.

Madhi, S.A., Baillie, V., Cutland, C.L., Voysey, M., Koen, A.L., Fairlie, L., Padayachee, S.D., Dheda, K., Barnabas, S.L., Bhorat, Q.E., et al. (2021). Efficacy of the ChAdOx1 nCoV-

19 Covid-19 Vaccine against the B.1.351 Variant. N. Engl. J. Med. 384, 1885-1898.

McCallum, M., Bassi, J., De Marco, A., Chen, A., Walls, A.C., Di Iulio, J., Alejandra Tortorici, M., Navarro, M.-J., Silacci-Fregni, C., Agostini, M., et al. (2021). SARS-CoV-2 immune evasion by variant B.1.427/B.1.429. BioRxiv https://doi.org/10.1101/2021.03.31.437925

McCoy, A.J., Grosse-Kunstleve, R.W., Adams, P.D., Winn, M.D., Storoni, L.C., and Read, R.J. (2007). Phaser crystallographic software. J. Appl. Crystallogr. 40, 658–674.

Nie, J., Li, Q., Wu, J., Zhao, C., Hao, H., Liu, H., Zhang, L., Nie, L., Qin, H., Wang, M., et al. (2020). Establishment and validation of a pseudovirus neutralization assay for SARS-CoV-2. Emerg. Microbes Infect. 9, 680–686.

Pinto, D., Park, Y.J., Beltramello, M., Walls, A.C., Tortorici, M.A., Bianchi, S., Jaconi, S., Culap, K., Zatta, F., De Marco, A., et al. (2020). Cross-neutralization of SARS-CoV-2 by a human monoclonal SARS-CoV antibody. Nature 583, 290–295.

Polack, F.P., Thomas, S.J., Kitchin, N., Absalon, J., Gurtman, A., Lockhart, S., Perez, J.L., Pérez Marc, G., Moreira, E.D., Zerbini, C., et al. (2020). Safety and Efficacy of the BNT162b2 mRNA Covid-19 Vaccine. N. Engl. J. Med. 383, 2603–2615.

Rambaut, A., Loman, N., Pybus, O., Barclay, W., Barrett, J., Carabelli, A., Connor, T., Peacock, T., Robertson, David, L., and Volz, E. (2020). Preliminary genomic characterisation of an emergent SARS-CoV-2 lineage in the UK defined by a novel set of spike mutations. [online] Available at: <https://virological.org/t/preliminary-genomic-characterisation-of-an-emergent-sars-cov-2-lineage-in-the-uk-defined-by-a-novel-set-of-spike-mutations/563> [Accessed 20 May 2021].

Robson, F., Khan, K.S., Le, T.K., Paris, C., Demirbag, S., Barfuss, P., Rocchi, P., and Ng, W.L. (2020). Coronavirus RNA Proofreading: Molecular Basis and Therapeutic Targeting. Mol. Cell 79, 710–727.

Seemann, T., Lane, C.R., Sherry, N.L., Duchene, S., Gonçalves da Silva, A., Caly, L., Sait, M., Ballard, S.A., Horan, K., Schultz, M.B., et al. (2020). Tracking the COVID-19 pandemic in Australia using genomics. Nat. Commun. 11, 1–9.

Shinde, V., Bhikha, S., Hoosain, Z., Archary, M., Bhorat, Q., Fairlie, L., Lalloo, U., Masilela, M.S.L., Moodley, D., Hanley, S., et al. (2021). Efficacy of NVX-CoV2373 Covid-19 Vaccine against the B.1.351 Variant. N. Engl. J. Med. 384, 1899-1909.

Skelly, D.T., Harding, A.C., Gilbert-Jaramillo, J. et al. (2021) Natural and vaccine-induced antibody and cellular responses against emerging SARS-CoV-2 variants of concern, PREPRINT (Version 1) available at Research Square [https://doi.org/10.21203/rs.3.rs-224655/v1]

Smith, D.J., Lapedes, A.S., De Jong, J.C., Bestebroer, T.M., Rimmelzwaan, G.F., Osterhaus, A.D.M.E., and Fouchier, R.A.M. (2004). Mapping the antigenic and genetic evolution of influenza virus. Science 305, 371–376.

Stuart, D.I., Levine, M., Muirhead, H., and Stammers, D.K. (1979). Crystal structure of cat muscle pyruvate kinase at a resolution of 2.6 Å. J. Mol. Biol. 134, 109–142.

Supasa, P., Zhou, D., Dejnirattisai, W., Liu, C., Mentzer, A.J., Ginn, H.M., Zhao, Y., Duyvesteyn, H.M.E., Nutalai, R., Tuekprakhon, A., et al. (2021). Reduced neutralization of SARS-CoV-2 B.1.1.7 variant by convalescent and vaccine sera. Cell 184, 2201-2211.

Tegally, H., Wilkinson, E., Lessells, R.J., Giandhari, J., Pillay, S., Msomi, N., Mlisana, K.,

Bhiman, J.N., von Gottberg, A., Walaza, S., et al. (2021). Sixteen novel lineages of SARS-CoV-2 in South Africa. Nat. Med. 27, 440-446.

Temperton, N.J. (2010). The use of retroviral pseudotypes for the measurement of antibody responses to SARS coronavirus. In Molecular Biology of the SARS-Coronavirus, (Springer Berlin Heidelberg), pp. 279–288.

Volz, E., Hill, V., McCrone, J.T., Price, A., Jorgensen, D., O'Toole, Á., Southgate, J., Johnson, R., Jackson, B., Nascimento, F.F., et al. (2021). Evaluating the Effects of SARS-CoV-2 Spike Mutation D614G on Transmissibility and Pathogenicity. Cell 184, 64-75.e11.

Voysey, M., Clemens, S.A.C., Madhi, S.A., Weckx, L.Y., Folegatti, P.M., Aley, P.K., Angus, B., Baillie, V.L., Barnabas, S.L., Bhorat, Q.E., et al. (2020). Safety and efficacy of the ChAdOx1 nCoV-19 vaccine (AZD1222) against SARS-CoV-2: an interim analysis of four randomised controlled trials in Brazil, South Africa, and the UK. Lancet 397, 99-111.

Walter, T.S., Diprose, J., Brown, J., Pickford, M., Owens, R.J., Stuart, D.I., and Harlos, K. (2003). A procedure for setting up high-throughput nanolitre crystallization experiments. I. Protocol design and validation. J. Appl. Crystallogr. *36*, 308–314.

Wang, P., Nair, M.S., Liu, L., Iketani, S., Luo, Y., Guo, Y., Wang, M., Yu, J., Zhang, B., Kwong, P.D., et al. (2021). Antibody Resistance of SARS-CoV-2 Variants B.1.351 and B.1.1.7. Nature 593, 130-135.

Winter, G. (2010). Xia2: An expert system for macromolecular crystallography data reduction. J. Appl. Crystallogr. 43, 186–190.

Winter, G., Waterman, D.G., Parkhurst, J.M., Brewster, A.S., Gildea, R.J., Gerstel, M., Fuentes-Montero, L., Vollmar, M., Michels-Clark, T., Young, I.D., et al. (2018). *DIALS* :

implementation and evaluation of a new integration package. Acta Crystallogr. Sect. D Struct. Biol. 74, 85–97.

Yuan, M., Liu, H., Wu, N.C., Lee, C.C.D., Zhu, X., Zhao, F., Huang, D., Yu, W., Hua, Y., Tien, H., et al. (2020). Structural basis of a shared antibody response to SARS-CoV-2. Science 369, 1119–1123.

Zahradník, J., Marciano, S., Shemesh, M., Zoler, E., Chiaravalli, J., Meyer, B., Dym, O., Elad, N., and Schreiber, G. (2021). SARS-CoV-2 RBD in vitro evolution follows contagious mutation spread, yet generates an able infection inhibitor. BioRxiv https://doi.org/10.1101/2021.01.06.425392.

Zhou, D., Dejnirattisai, W., Supasa, P., Liu, C., Mentzer, A.J., Ginn, H.M., Zhao, Y., Duyvesteyn, H.M.E., Tuekprakhon, A., Nutalai, R., et al. (2021). Evidence of escape of SARS-CoV-2 variant B.1.351 from natural and vaccine induced sera. Cell 184, 2348-2361.

Highlights:

- **Vaccine/convalescent sera show reduced neutralization of B.1.617.1 and B.1.617.2**
- **Sera from B.1.351and P.1 show markedly reduced neutralization of B.1.617.2**
- **B.1.351, P.1 and B.1.617.2 are antigenically divergent**
- **Vaccines based on B.1.1.7 may broadly protect against current variants**

The B.1.617 lineage of SARS-CoV-2, especially the delta strain that is B.1.617.2 has contributed to the wave of infection in the Indian subcontinent. Structural and serological analyses show no evidence of antibody escape but individuals previously infected with either the B.1.351 (beta) and P.1 (gamma) variants are likely more susceptible to reinfection by the delta strain. Vaccines based on B.1.1.7 (alpha) are likely to provide the broadest protection against current variants.

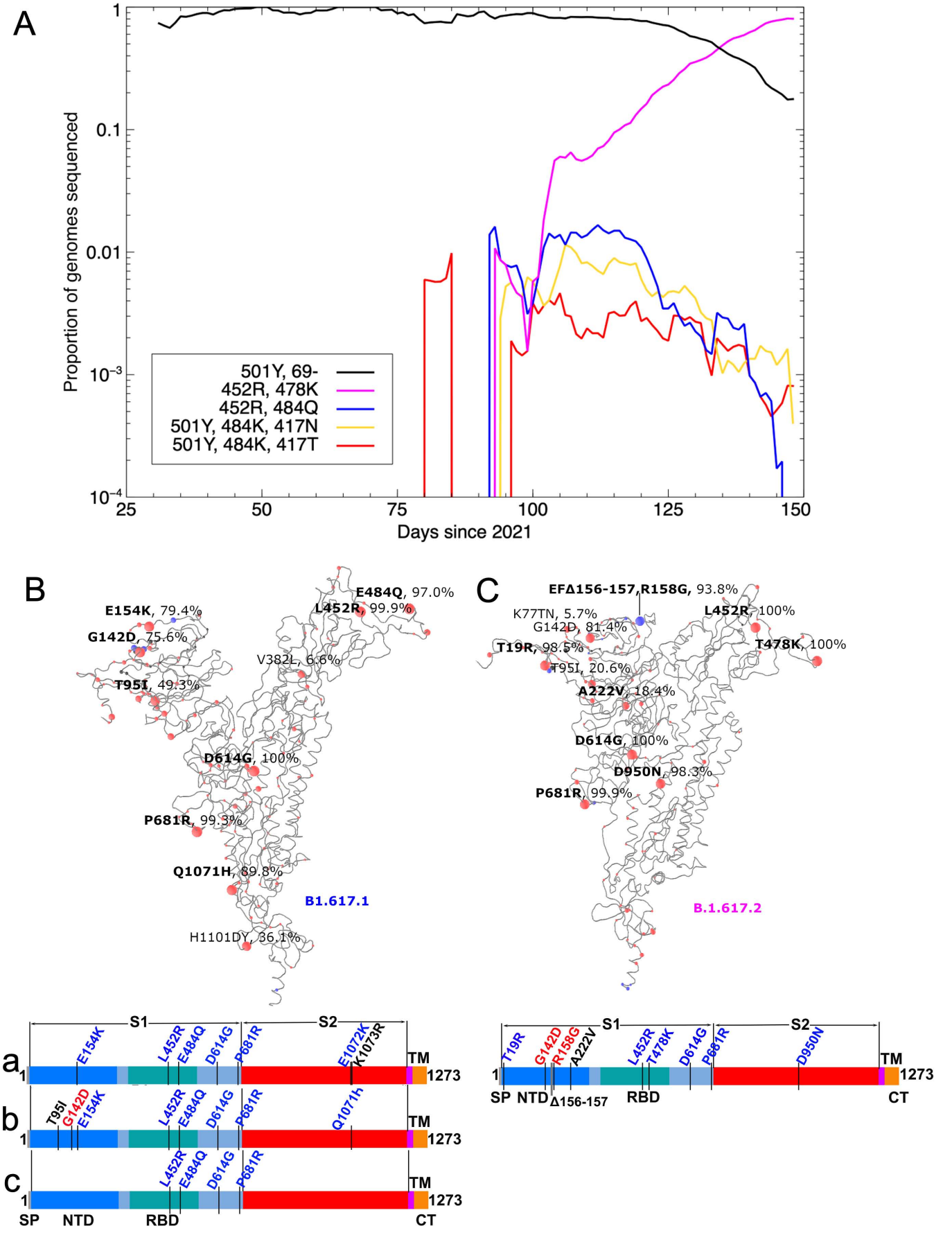
A
Proportion of genomes sequenced
Days since 2021
501Y, 69-
452R, 478K
452R, 484Q
501Y, 484K, 417N
501Y, 484K, 417T
B
E484Q, 97.0%
L452R, 99.9%
E154K, 79.4%
G142D, 75.6%
V382L, 6.6%
T95I, 49.3%
D614G, 100%
P681R, 99.3%
Q1071H, 89.8%
B1.617.1
H1101DY, 36.1%
C
EFΔ156-157,R158G, 93.8%
K77TN, 5.7%
G142D, 81.4%
L452R, 100%
T19R, 98.5%
T478K, 100%
T95I, 20.6%
A222V, 18.4%
D614G, 100%
D950N, 98.3%
P681R, 99.9%
B.1.617.2
S1
S2
TM
SP
NTD
RBD
CT
Δ156-157

Figure 1

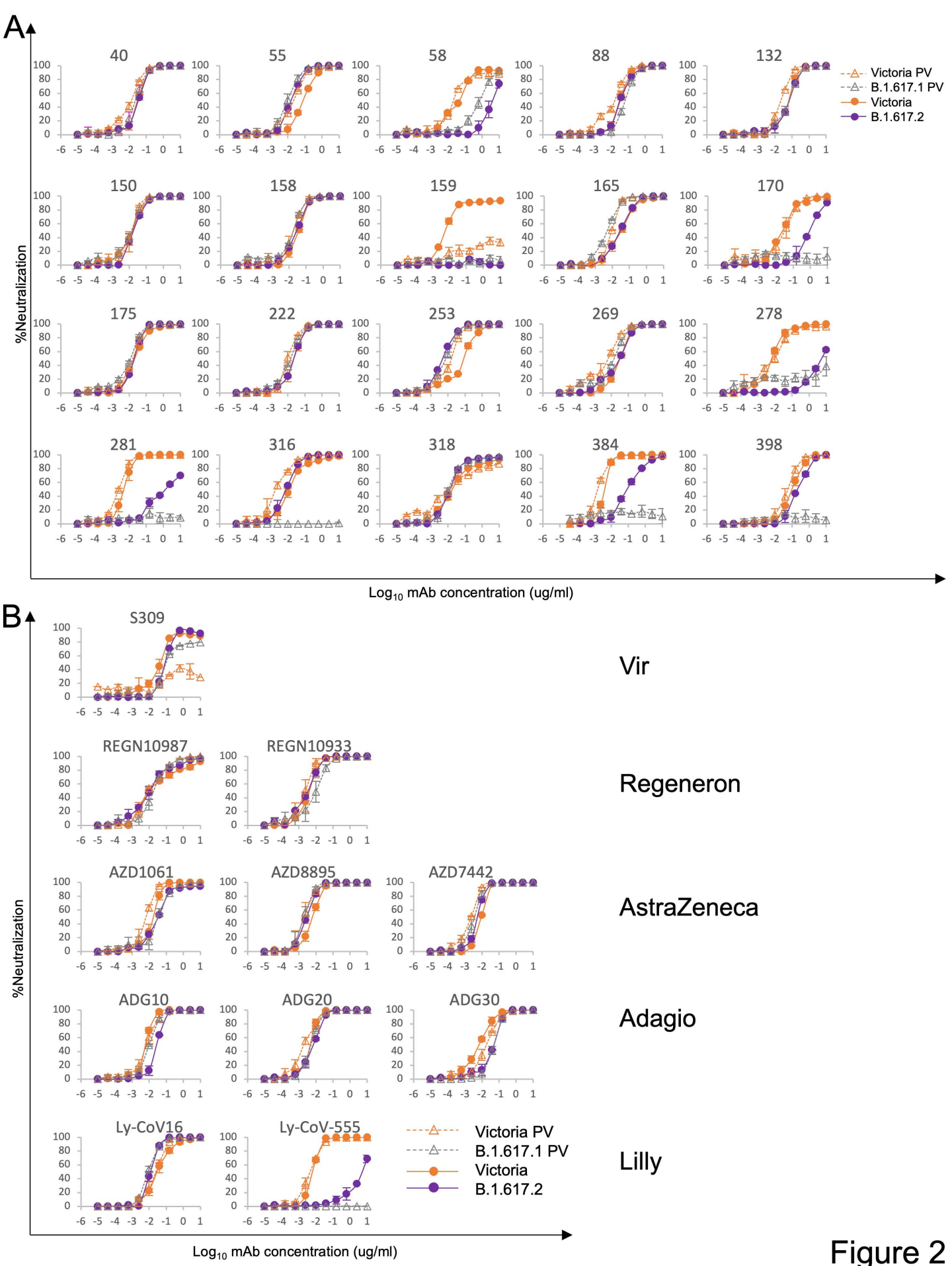
A
40
55
58
88
132
150
158
159
165
170
175
222
253
269
278
281
316
318
384
398
Victoria PV
B.1.617.1 PV
Victoria
B.1.617.2
%Neutralization
Log10 mAb concentration (ug/ml)
B
S309
Vir
REGN10987
REGN10933
Regeneron
AZD1061
AZD8895
AZD7442
AstraZeneca
ADG10
ADG20
ADG30
Adagio
Ly-CoV16
Ly-CoV-555
Lilly
Victoria PV
B.1.617.1 PV
Victoria
B.1.617.2
%Neutralization
Log10 mAb concentration (ug/ml)

Figure 2

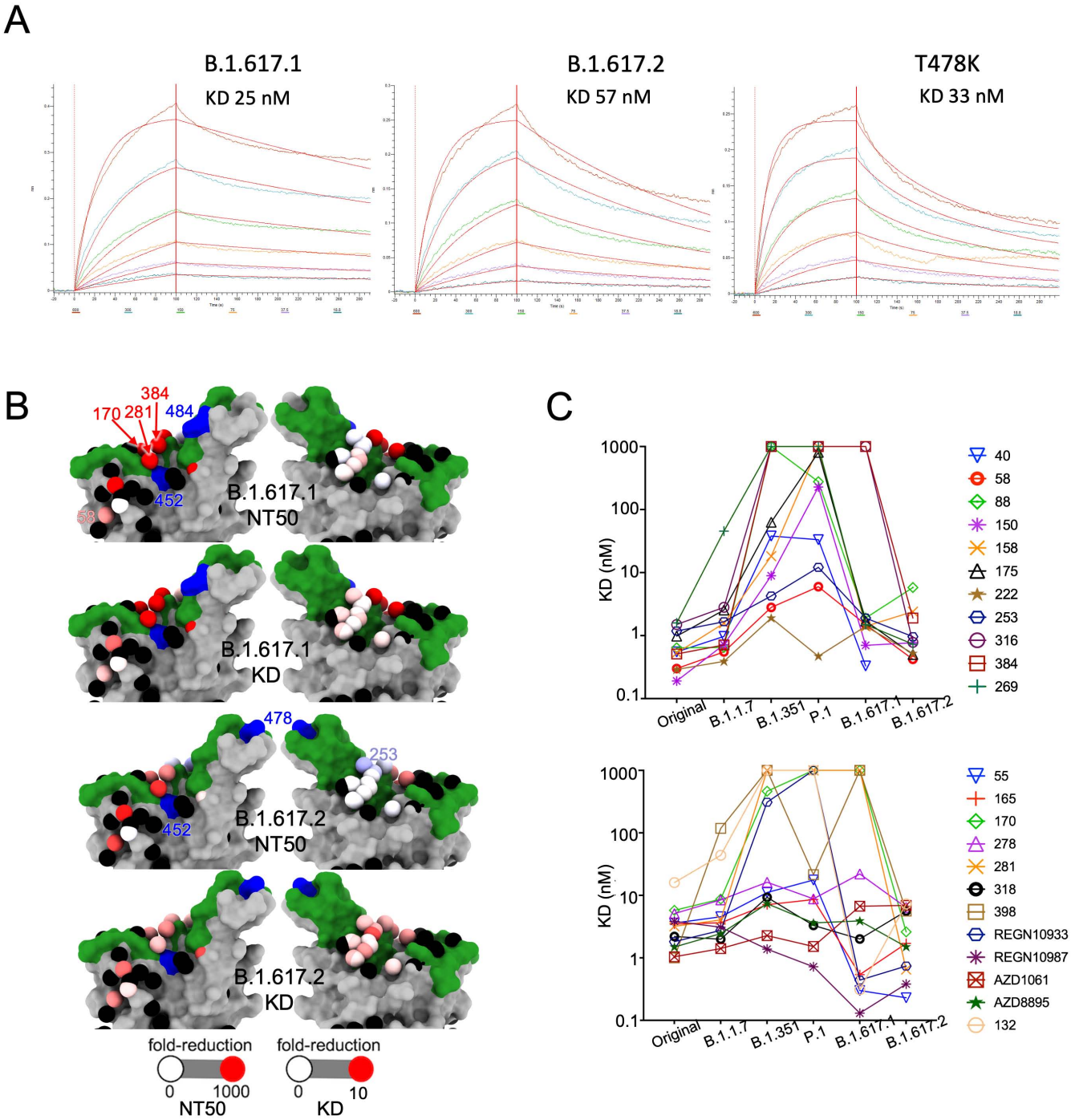
A
B.1.617.1
KD 25 nM
B.1.617.2
KD 57 nM
T478K
KD 33 nM
B
384
170
281
484
452
58
B.1.617.1
NT50
B.1.617.1
KD
478
253
452
B.1.617.2
NT50
B.1.617.2
KD
fold-reduction
0
1000
NT50
fold-reduction
0
10
KD
C
KD (nM)
1000
100
10
1
0.1
Original
B.1.1.7
B.1.351
P.1
B.1.617.1
B.1.617.2
40
58
88
150
158
175
222
253
316
384
269
KD (nM)
1000
100
10
1
0.1
Original
B.1.1.7
B.1.351
P.1
B.1.617.1
B.1.617.2
55
165
170
278
281
318
398
REGN10933
REGN10987
AZD1061
AZD8895
132

Figure 3

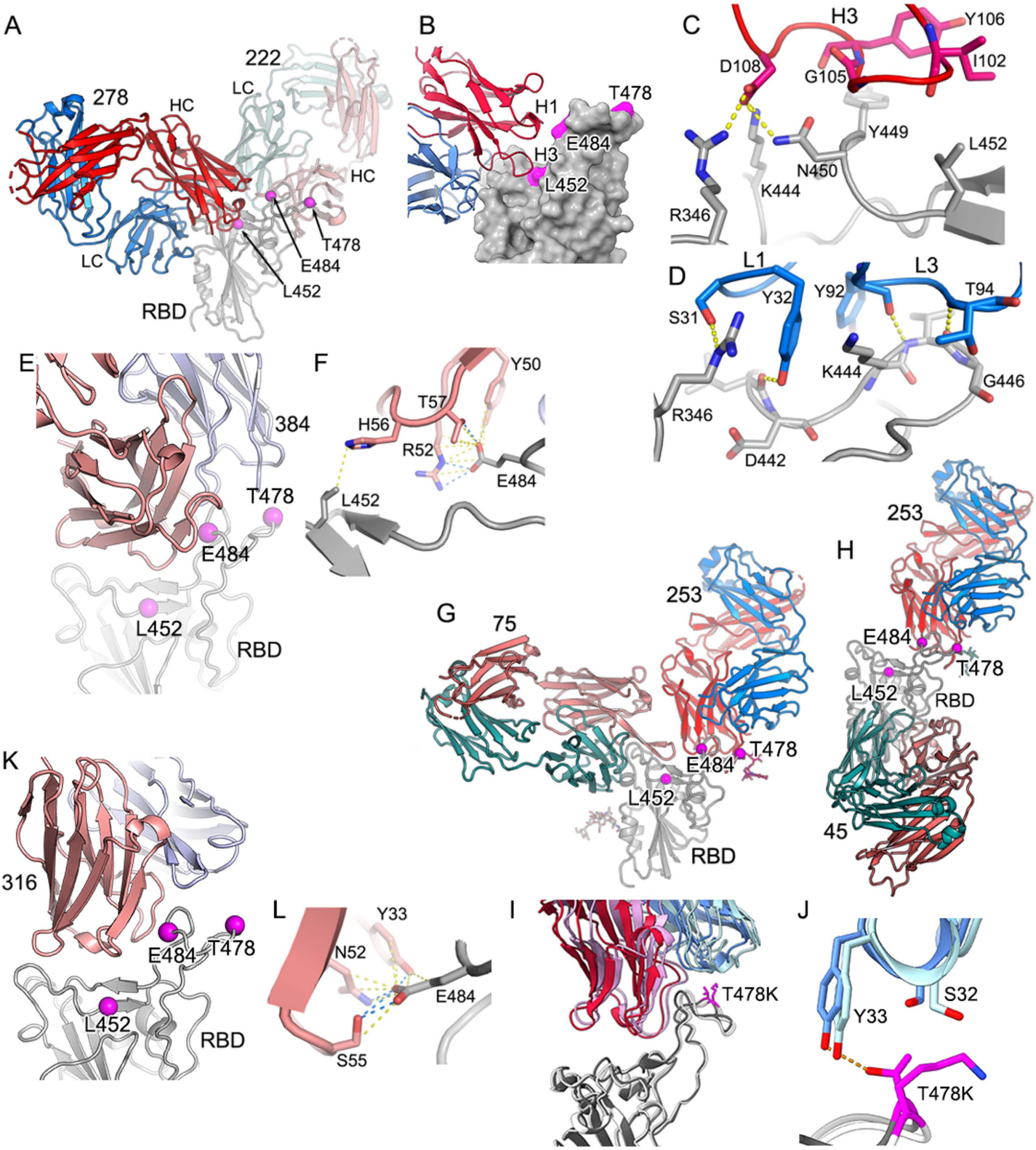
A
278
HC
222
LC
LC
HC
T478
E484
L452
RBD
B
H1
T478
E484
H3
L452
C
H3
Y106
D108
G105
I102
Y449
L452
N450
K444
R346
D
L1
L3
Y32
Y92
T94
S31
K444
G446
R346
D442
E
384
T478
E484
L452
RBD
F
Y50
T57
H56
R52
E484
L452
G
75
253
T478
E484
L452
RBD
H
253
E484
T478
L452
RBD
45
K
316
E484
T478
L452
RBD
L
Y33
N52
E484
S55
I
T478K
J
S32
Y33
T478K

Figure 4

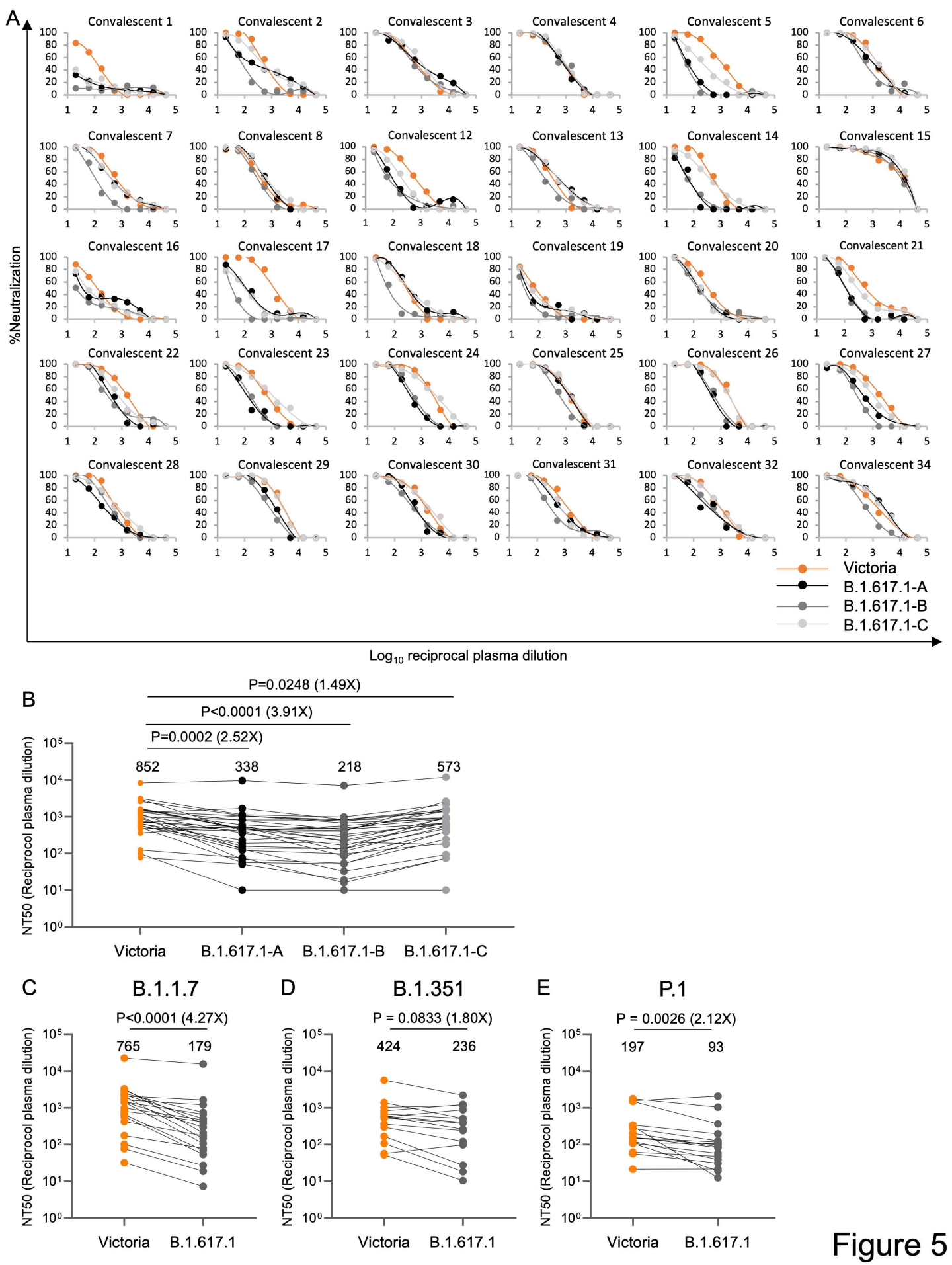
A
Convalescent 1
Convalescent 2
Convalescent 3
Convalescent 4
Convalescent 5
Convalescent 6
Convalescent 7
Convalescent 8
Convalescent 12
Convalescent 13
Convalescent 14
Convalescent 15
Convalescent 16
Convalescent 17
Convalescent 18
Convalescent 19
Convalescent 20
Convalescent 21
Convalescent 22
Convalescent 23
Convalescent 24
Convalescent 25
Convalescent 26
Convalescent 27
Convalescent 28
Convalescent 29
Convalescent 30
Convalescent 31
Convalescent 32
Convalescent 34
%Neutralization
Victoria
B.1.617.1-A
B.1.617.1-B
B.1.617.1-C
Log10 reciprocal plasma dilution
B
P=0.0248 (1.49X)
P<0.0001 (3.91X)
P=0.0002 (2.52X)
852
338
218
573
NT50 (Reciprocol plasma dilution)
Victoria
B.1.617.1-A
B.1.617.1-B
B.1.617.1-C
C
B.1.1.7
P<0.0001 (4.27X)
765
179
Victoria
B.1.617.1
D
B.1.351
P = 0.0833 (1.80X)
424
236
Victoria
B.1.617.1
E
P.1
P = 0.0026 (2.12X)
197
93
Victoria
B.1.617.1

Figure 5

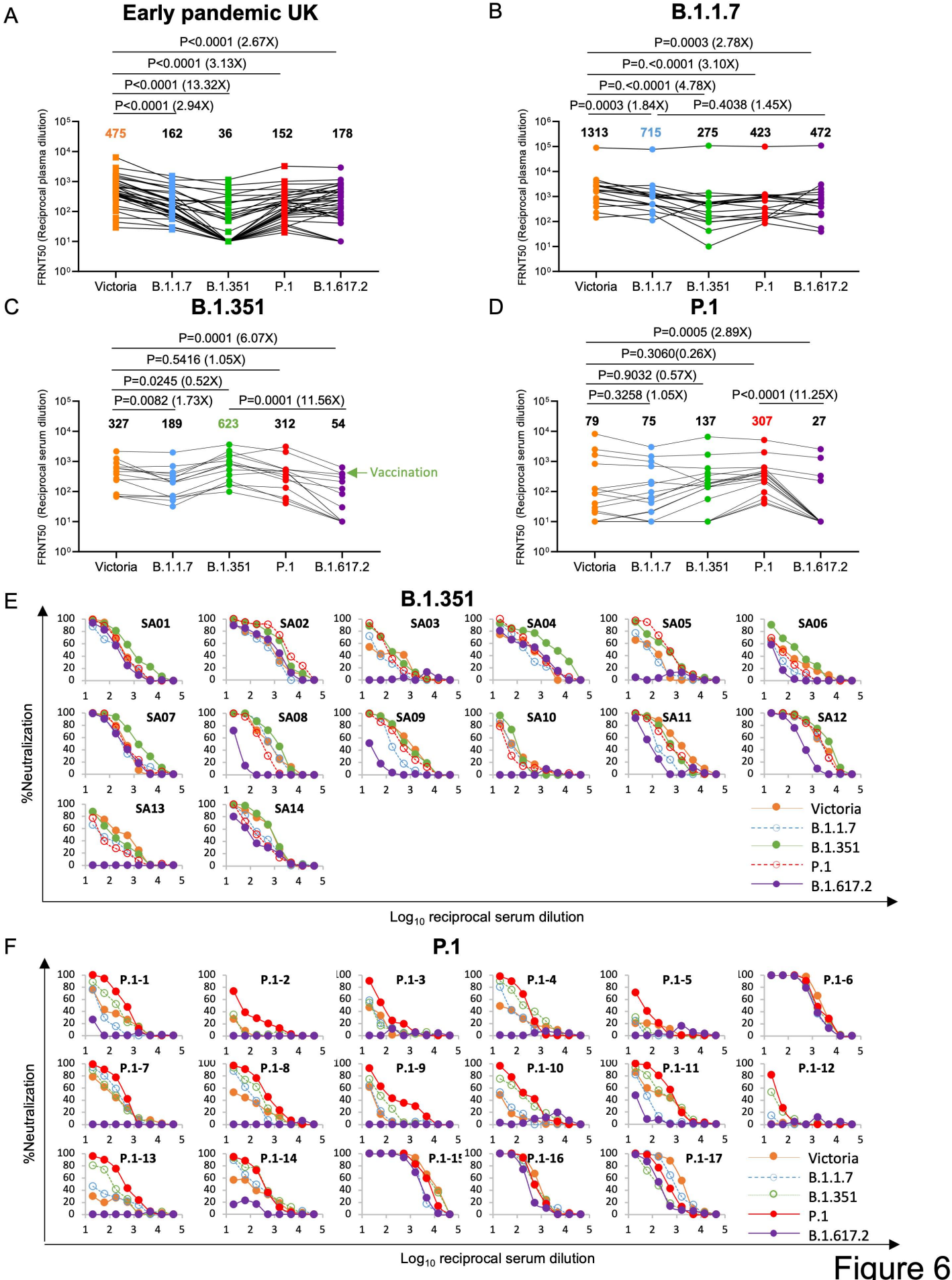
A
Early pandemic UK
P<0.0001 (2.67X)
P<0.0001 (3.13X)
P<0.0001 (13.32X)
P<0.0001 (2.94X)
475
162
36
152
178
FRNT50 (Reciprocal plasma dilution)
Victoria
B.1.1.7
B.1.351
P.1
B.1.617.2
B
B.1.1.7
P=0.0003 (2.78X)
P=0.<0.0001 (3.10X)
P=0.<0.0001 (4.78X)
P=0.0003 (1.84X)
P=0.4038 (1.45X)
1313
715
275
423
472
C
B.1.351
P=0.0001 (6.07X)
P=0.5416 (1.05X)
P=0.0245 (0.52X)
P=0.0082 (1.73X)
P=0.0001 (11.56X)
327
189
623
312
54
Vaccination
D
P.1
P=0.0005 (2.89X)
P=0.3060(0.26X)
P=0.9032 (0.57X)
P=0.3258 (1.05X)
P<0.0001 (11.25X)
79
75
137
307
27
E
B.1.351
SA01
SA02
SA03
SA04
SA05
SA06
SA07
SA08
SA09
SA10
SA11
SA12
SA13
SA14
%Neutralization
Victoria
B.1.1.7
B.1.351
P.1
B.1.617.2
Log10 reciprocal serum dilution
F
P.1
P.1-1
P.1-2
P.1-3
P.1-4
P.1-5
P.1-6
P.1-7
P.1-8
P.1-9
P.1-10
P.1-11
P.1-12
P.1-13
P.1-14
P.1-15
P.1-16
P.1-17
%Neutralization
Victoria
B.1.1.7
B.1.351
P.1
B.1.617.2
Log10 reciprocal serum dilution

Figure 6

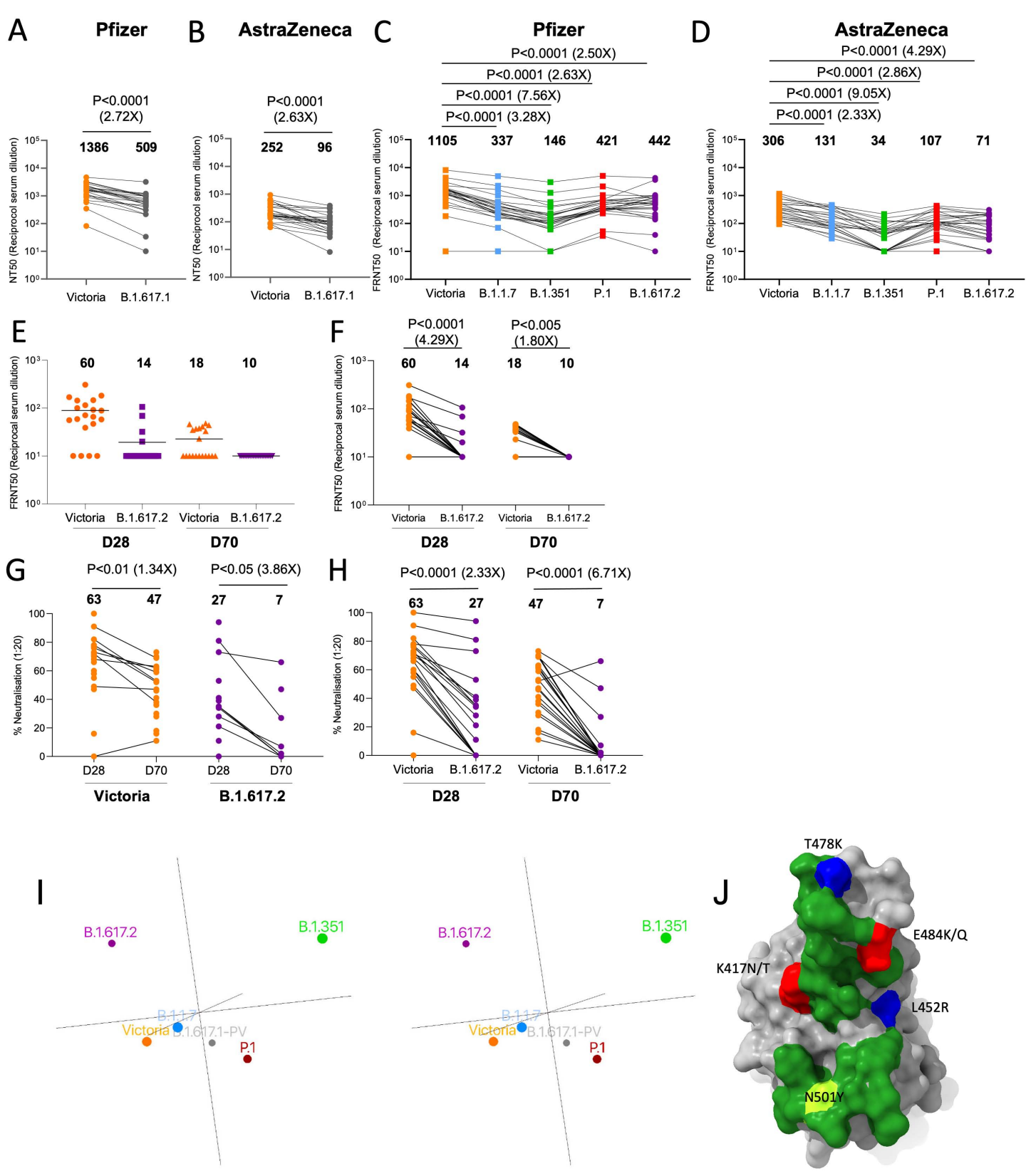
A
Pfizer
P<0.0001
(2.72X)
1386
509
NT50 (Reciprocol serum dilution)
Victoria
B.1.617.1
B
AstraZeneca
P<0.0001
(2.63X)
252
96
NT50 (Reciprocol serum dilution)
Victoria
B.1.617.1
C
Pfizer
P<0.0001 (2.50X)
P<0.0001 (2.63X)
P<0.0001 (7.56X)
P<0.0001 (3.28X)
1105
337
146
421
442
FRNT50 (Reciprocal serum dilution)
Victoria
B.1.1.7
B.1.351
P.1
B.1.617.2
D
AstraZeneca
P<0.0001 (4.29X)
P<0.0001 (2.86X)
P<0.0001 (9.05X)
P<0.0001 (2.33X)
306
131
34
107
71
FRNT50 (Reciprocal serum dilution)
Victoria
B.1.1.7
B.1.351
P.1
B.1.617.2
E
60
14
18
10
FRNT50 (Reciprocal serum dilution)
Victoria
B.1.617.2
Victoria
B.1.617.2
D28
D70
F
P<0.0001
(4.29X)
P<0.005
(1.80X)
60
14
18
10
FRNT50 (Reciprocal serum dilution)
Victoria
B.1.617.2
Victoria
B.1.617.2
D28
D70
G
P<0.01 (1.34X)
P<0.05 (3.86X)
63
47
27
7
% Neutralisation (1:20)
D28
D70
D28
D70
Victoria
B.1.617.2
H
P<0.0001 (2.33X)
P<0.0001 (6.71X)
63
27
47
7
% Neutralisation (1:20)
Victoria
B.1.617.2
Victoria
B.1.617.2
D28
D70
I
B.1.617.2
B.1.351
B.1.1.7
Victoria
B.1.617.1-PV
P.1
B.1.617.2
B.1.351
B.1.1.7
Victoria
B.1.617.1-PV
P.1
J
T478K
E484K/Q
K417N/T
L452R
N501Y

Figure 7

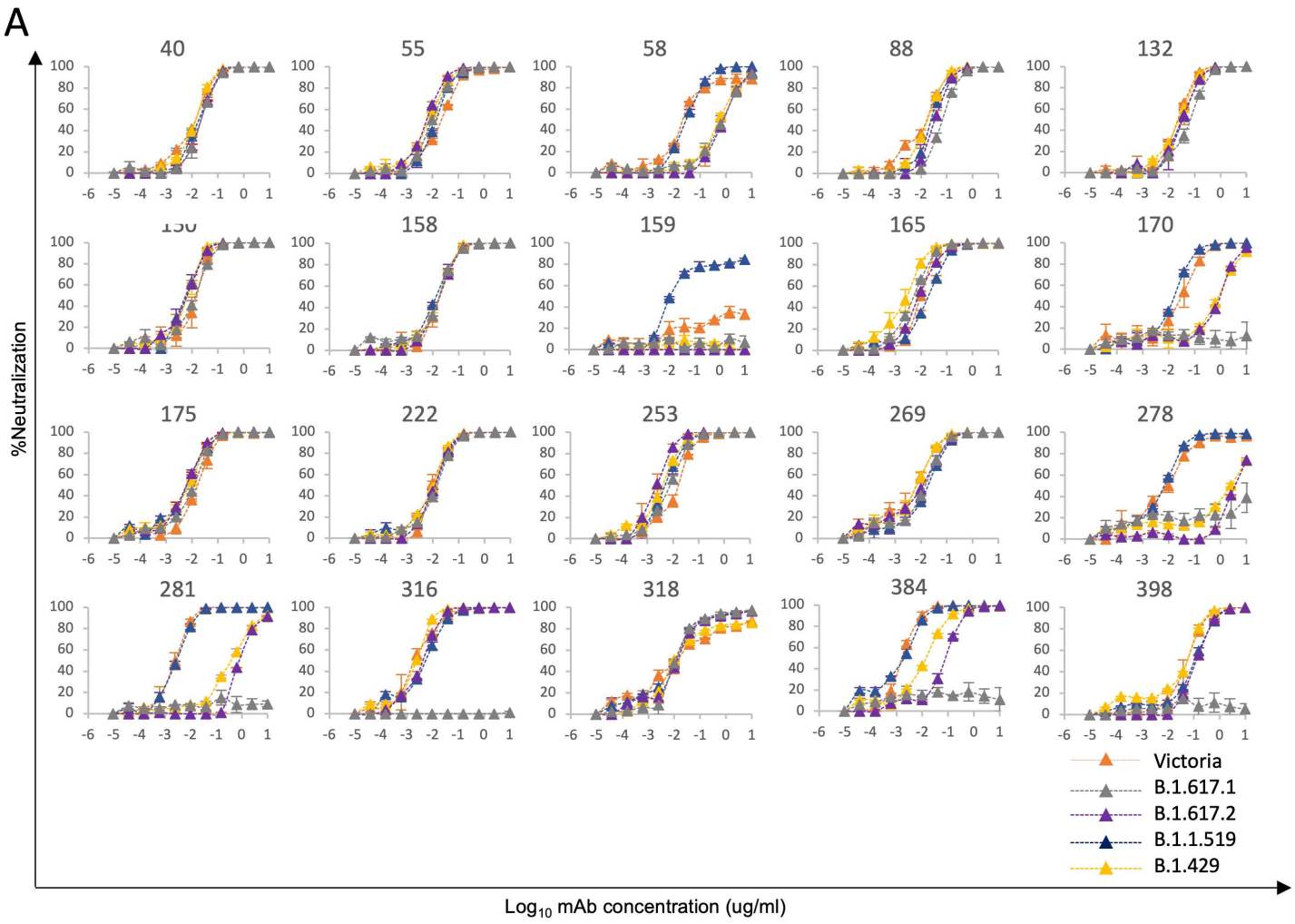
A
40
55
58
88
132
150
158
159
165
170
175
222
253
269
278
281
316
318
384
398
%Neutralization
Log10 mAb concentration (ug/ml)
Victoria
B.1.617.1
B.1.617.2
B.1.1.519
B.1.429

Figure S1

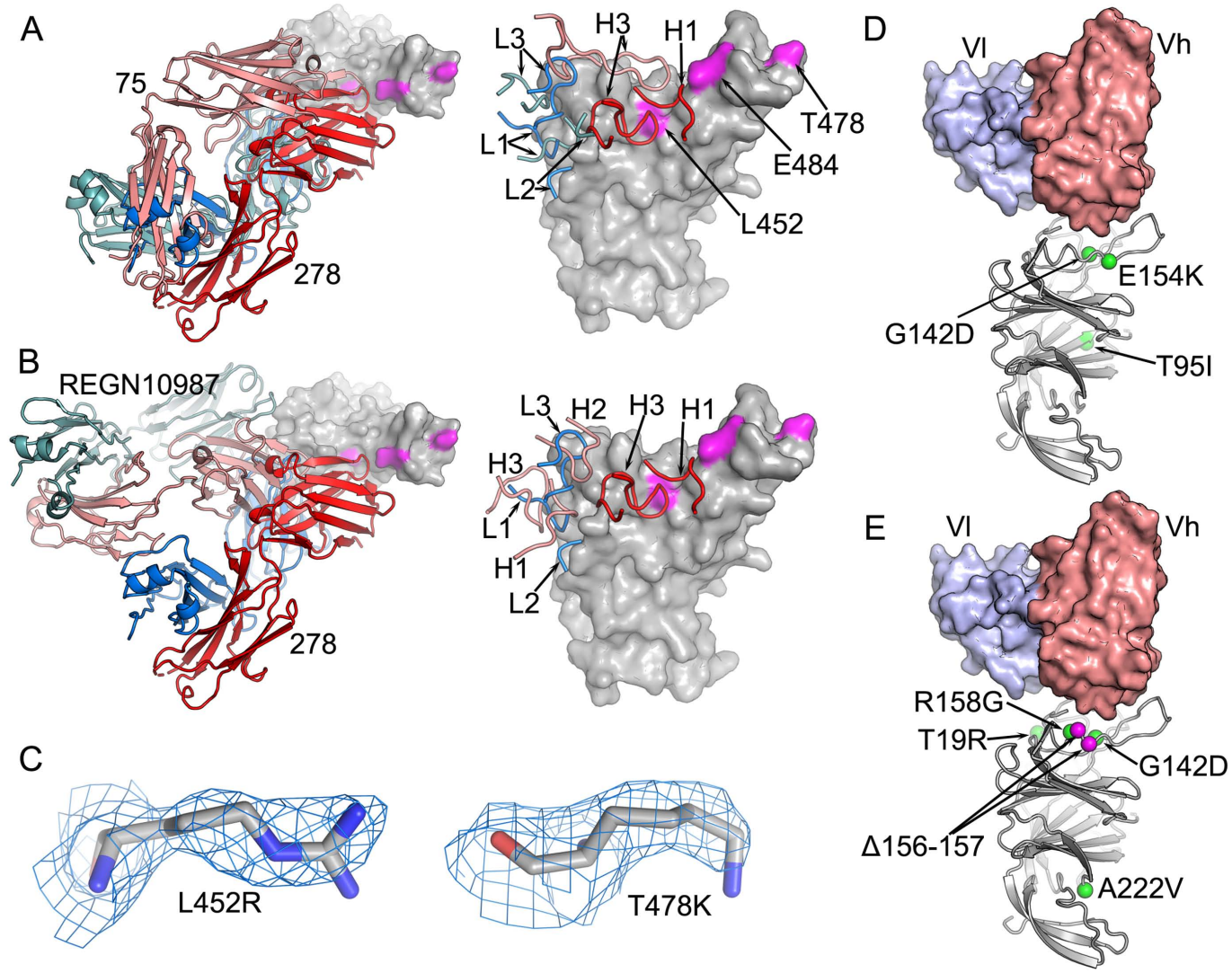
A
75
278
L3
H3
H1
T478
L1
E484
L2
L452
B
REGN10987
278
L3
H2
H3
H1
H3
L1
H1
L2
C
L452R
T478K
D
Vl
Vh
E154K
G142D
T95I
E
Vl
Vh
R158G
T19R
G142D
Δ156-157
A222V

Figure S2

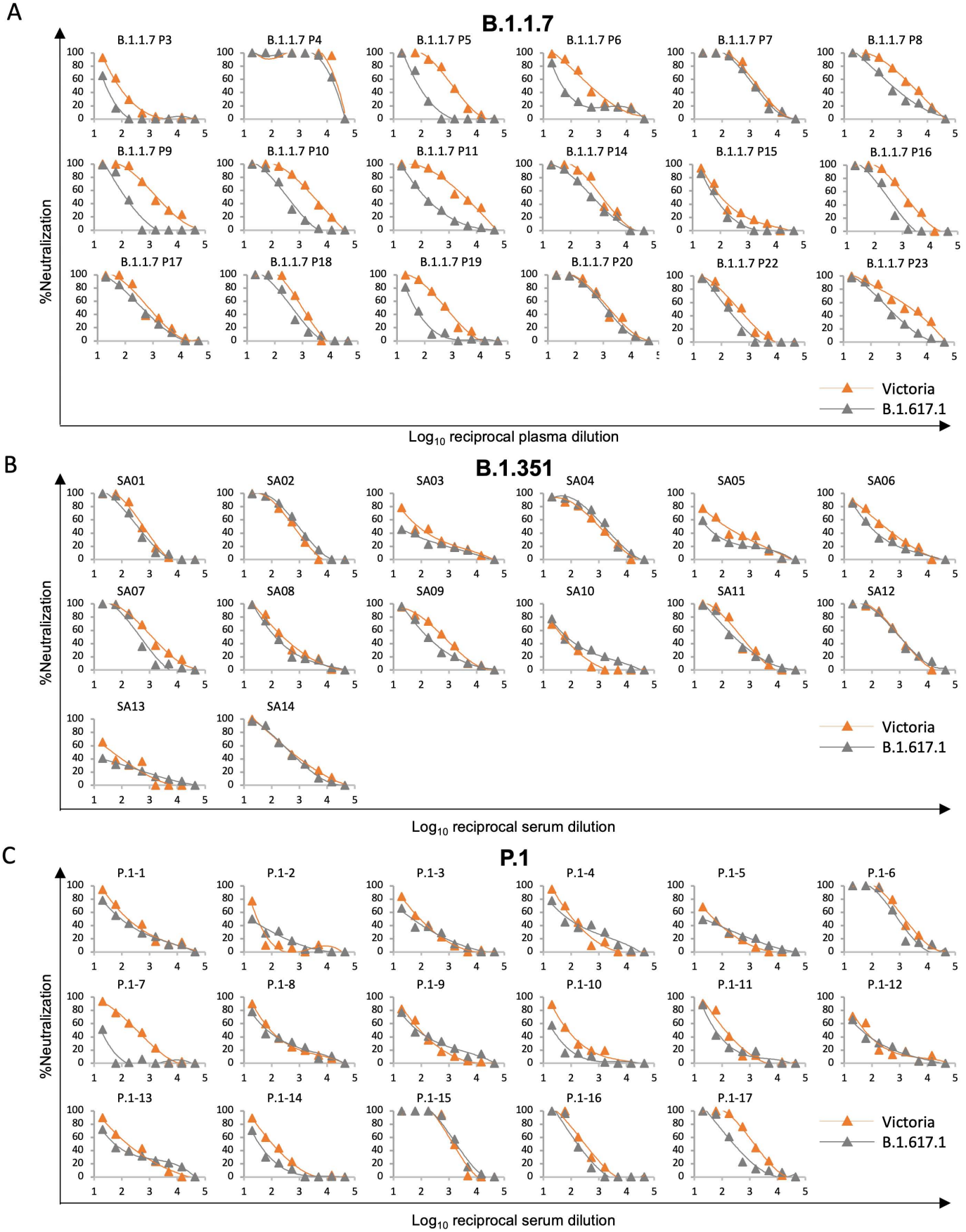
A
B.1.1.7
B.1.1.7 P3
B.1.1.7 P4
B.1.1.7 P5
B.1.1.7 P6
B.1.1.7 P7
B.1.1.7 P8
B.1.1.7 P9
B.1.1.7 P10
B.1.1.7 P11
B.1.1.7 P14
B.1.1.7 P15
B.1.1.7 P16
B.1.1.7 P17
B.1.1.7 P18
B.1.1.7 P19
B.1.1.7 P20
B.1.1.7 P22
B.1.1.7 P23
%Neutralization
Victoria
B.1.617.1
Log10 reciprocal plasma dilution
B
B.1.351
SA01
SA02
SA03
SA04
SA05
SA06
SA07
SA08
SA09
SA10
SA11
SA12
SA13
SA14
%Neutralization
Victoria
B.1.617.1
Log10 reciprocal serum dilution
C
P.1
P.1-1
P.1-2
P.1-3
P.1-4
P.1-5
P.1-6
P.1-7
P.1-8
P.1-9
P.1-10
P.1-11
P.1-12
P.1-13
P.1-14
P.1-15
P.1-16
P.1-17
%Neutralization
Victoria
B.1.617.1
Log10 reciprocal serum dilution

Figure S3

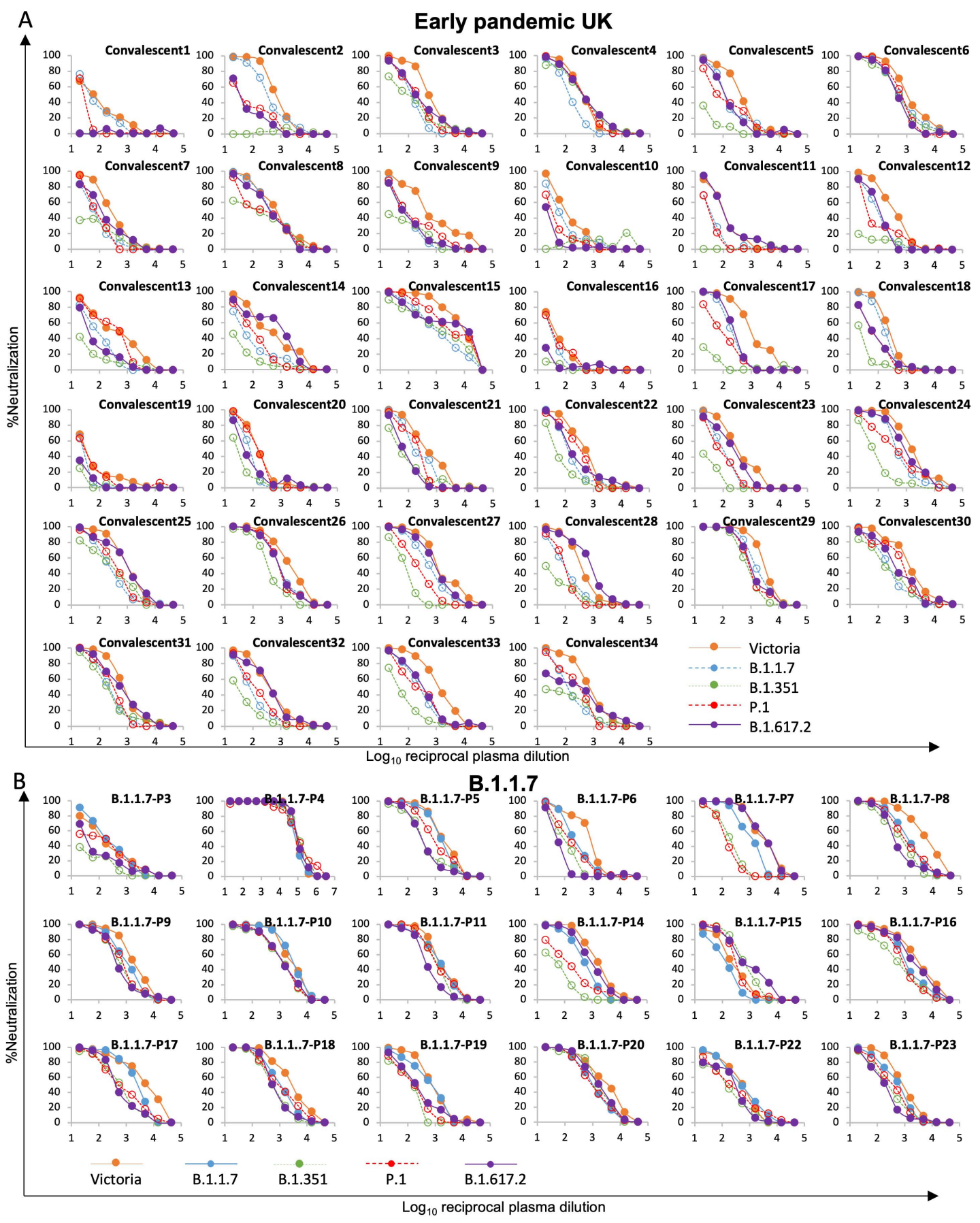
A
Early pandemic UK
Convalescent1
Convalescent2
Convalescent3
Convalescent4
Convalescent5
Convalescent6
Convalescent7
Convalescent8
Convalescent9
Convalescent10
Convalescent11
Convalescent12
Convalescent13
Convalescent14
Convalescent15
Convalescent16
Convalescent17
Convalescent18
Convalescent19
Convalescent20
Convalescent21
Convalescent22
Convalescent23
Convalescent24
Convalescent25
Convalescent26
Convalescent27
Convalescent28
Convalescent29
Convalescent30
Convalescent31
Convalescent32
Convalescent33
Convalescent34
Victoria
B.1.1.7
B.1.351
P.1
B.1.617.2
%Neutralization
Log10 reciprocal plasma dilution
B
B.1.1.7
B.1.1.7-P3
B.1.1.7-P4
B.1.1.7-P5
B.1.1.7-P6
B.1.1.7-P7
B.1.1.7-P8
B.1.1.7-P9
B.1.1.7-P10
B.1.1.7-P11
B.1.1.7-P14
B.1.1.7-P15
B.1.1.7-P16
B.1.1.7-P17
B.1.1..7-P18
B.1.1.7-P19
B.1.1.7-P20
B.1.1.7-P22
B.1.1.7-P23
Victoria
B.1.1.7
B.1.351
P.1
B.1.617.2
%Neutralization
Log10 reciprocal plasma dilution

Figure S4

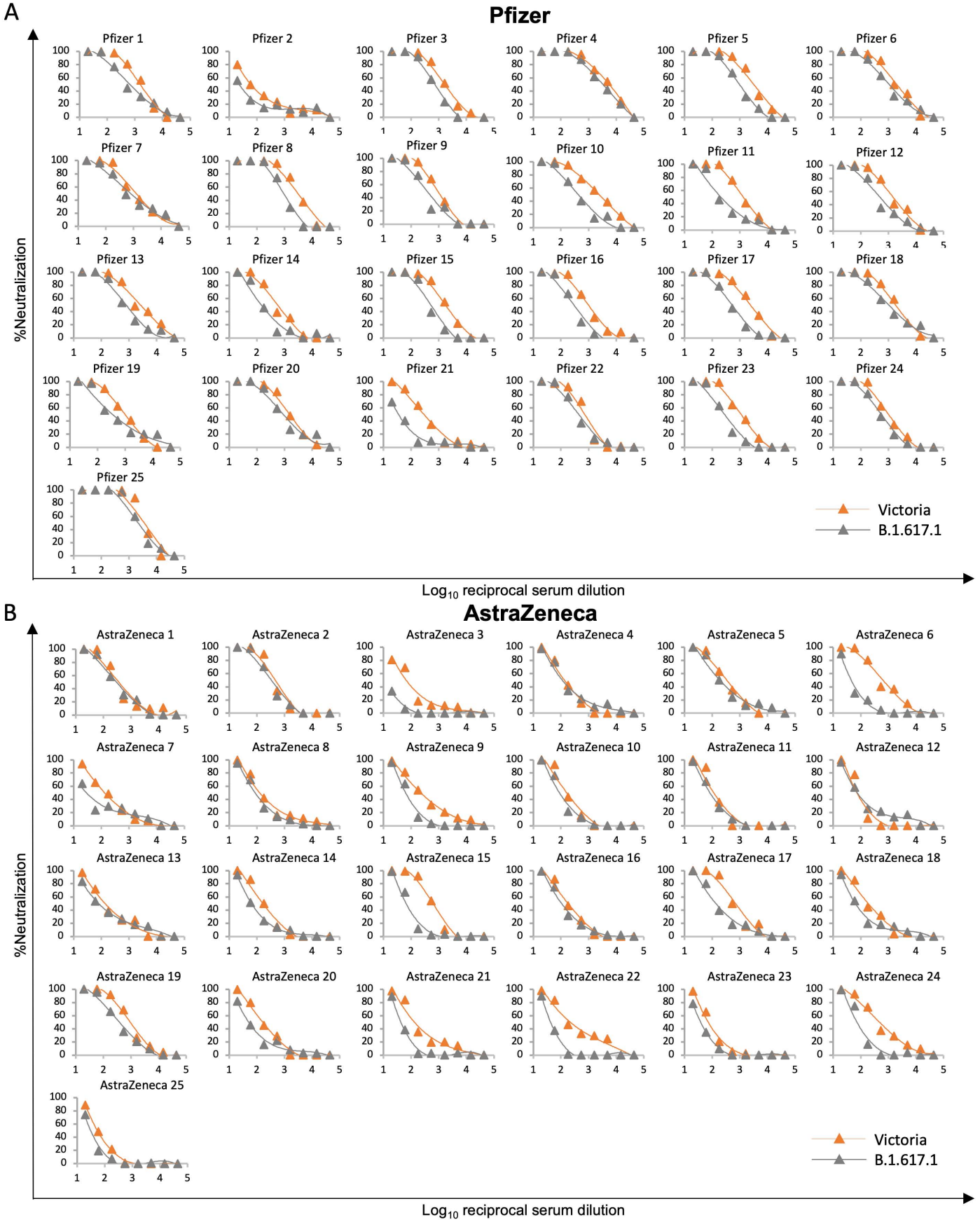
A
Pfizer
Pfizer 1
Pfizer 2
Pfizer 3
Pfizer 4
Pfizer 5
Pfizer 6
Pfizer 7
Pfizer 8
Pfizer 9
Pfizer 10
Pfizer 11
Pfizer 12
Pfizer 13
Pfizer 14
Pfizer 15
Pfizer 16
Pfizer 17
Pfizer 18
Pfizer 19
Pfizer 20
Pfizer 21
Pfizer 22
Pfizer 23
Pfizer 24
Pfizer 25
%Neutralization
Victoria
B.1.617.1
Log10 reciprocal serum dilution
B
AstraZeneca
AstraZeneca 1
AstraZeneca 2
AstraZeneca 3
AstraZeneca 4
AstraZeneca 5
AstraZeneca 6
AstraZeneca 7
AstraZeneca 8
AstraZeneca 9
AstraZeneca 10
AstraZeneca 11
AstraZeneca 12
AstraZeneca 13
AstraZeneca 14
AstraZeneca 15
AstraZeneca 16
AstraZeneca 17
AstraZeneca 18
AstraZeneca 19
AstraZeneca 20
AstraZeneca 21
AstraZeneca 22
AstraZeneca 23
AstraZeneca 24
AstraZeneca 25
%Neutralization
Victoria
B.1.617.1
Log10 reciprocal serum dilution

Figure S5

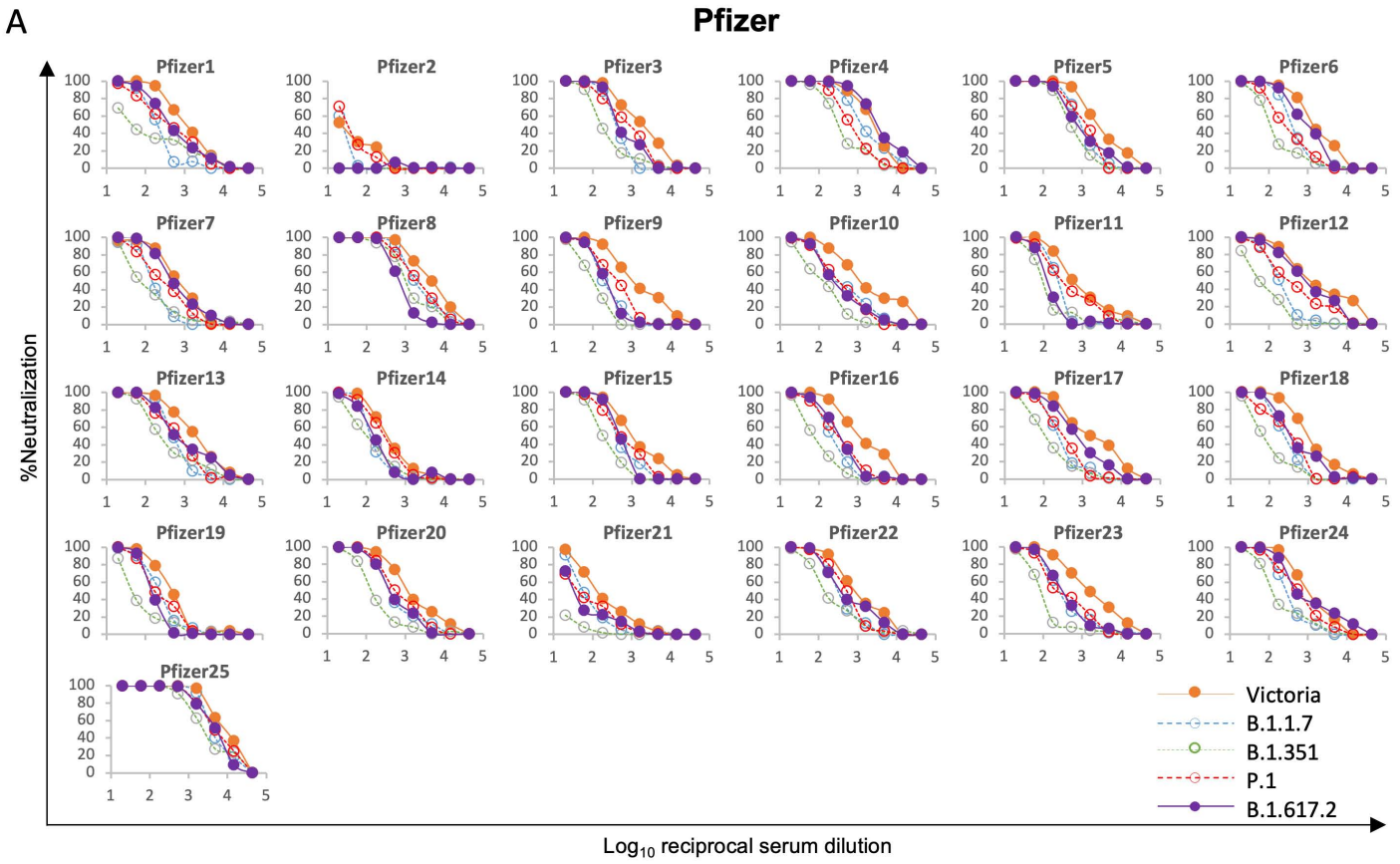
A
Pfizer
Pfizer1
Pfizer2
Pfizer3
Pfizer4
Pfizer5
Pfizer6
Pfizer7
Pfizer8
Pfizer9
Pfizer10
Pfizer11
Pfizer12
Pfizer13
Pfizer14
Pfizer15
Pfizer16
Pfizer17
Pfizer18
Pfizer19
Pfizer20
Pfizer21
Pfizer22
Pfizer23
Pfizer24
Pfizer25
%Neutralization
Log10 reciprocal serum dilution
Victoria
B.1.1.7
B.1.351
P.1
B.1.617.2

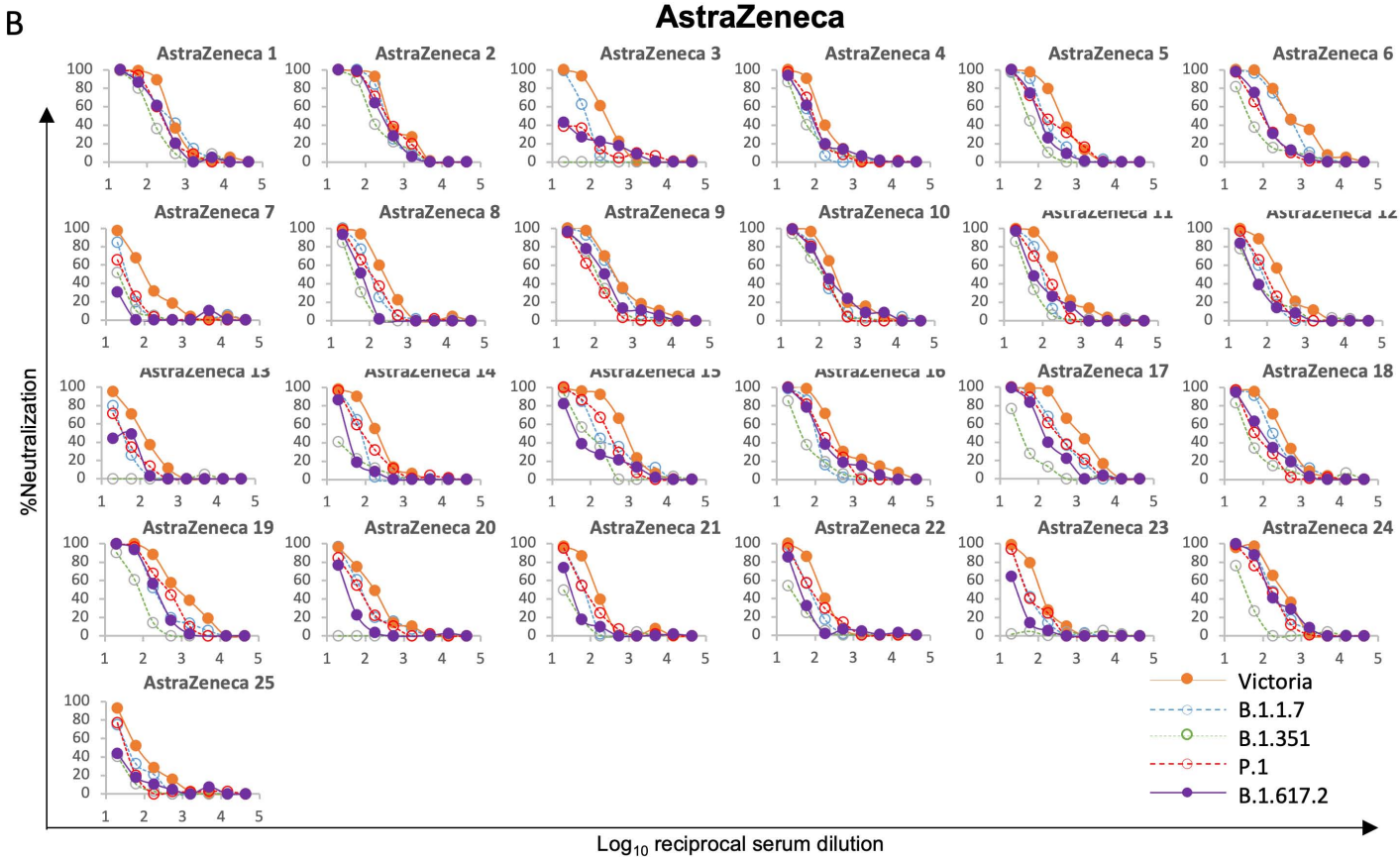
B
AstraZeneca
AstraZeneca 1
AstraZeneca 2
AstraZeneca 3
AstraZeneca 4
AstraZeneca 5
AstraZeneca 6
AstraZeneca 7
AstraZeneca 8
AstraZeneca 9
AstraZeneca 10
AstraZeneca 17
AstraZeneca 18
AstraZeneca 19
AstraZeneca 20
AstraZeneca 21
AstraZeneca 22
AstraZeneca 23
AstraZeneca 24
AstraZeneca 25
%Neutralization
Log10 reciprocal serum dilution
Victoria
B.1.1.7
B.1.351
P.1
B.1.617.2

Figure S6

Table S1. NT50 titres against pseudo typed lentiviruses expressing full-length spike of SARS-CoV-2 strains Victoria, B.1.617.1 , B.1.617.2, B.1.1.519 and B.1.429, live virus strains Victoria and B.1.617.2, and KD values for binding to different RBDs by BLI. (A) 20 human monoclonal antibodies (B) 11 human monoclonal antibodies in clinical trials. The data underpinning the Victoria live virus neutralization curves have been previously reported (Supasa et al, 2021). Related to Figure2.

mAb	IC50 (ug/ml)							FRNT50 ratio					KD (nM)					Immunoglobulin gene usage		
	Pseudovirus					Authentic virus		Pseudovirus				Authentic virus								
	Victoria	B.1.617.1	B.1.617.2	B.1.1.519	B.1.429	Victoria	B.1.617.2	B.1.617.1 /Victoria	B.1.617.2 /Victoria	B.1.1.519 /Victoria	B.1.429/ Victoria	B.1.617.2/ Victoria	Victor-ia RBD	RBD L452R	RBD T478K	RBD L452R, E484Q	RBD L452R, T478K	IGHV	K/λ	IGLV
40	0.008 ± 0.000	0.024 ± 0.008	0.024±0.002	0.017±0.002	0.011±0.000	0.026 ± 0.007	0.029 ± 0.010	3.0	2.8	2.1	1.4	1.1	0.34	0.50	0.16	0.33	0.47	3-66	K	1-33 or 1D-33
55	0.019 ± 0.002	0.010 ± 0.004	0.007±0.002	0.014±0.002	0.005±0.001	0.095 ± 0.015	0.016 ± 0.005	0.5	0.3	0.7	0.3	0.2	0.10	0.13	0.29	0.30	0.23	1-58	K	3-20
58	0.032 ± 0.005	0.690 ± 0.313	1.005±0.017	0.032±0.002	0.497±0.049	0.041 ± 0.003	6.434 ± 2.623	21.6	26.2	1.0	15.5	156.3	0.14	0.50	0.19	1.5	0.42	3-9	λ	3-21
88	0.010 ± 0.002	0.072 ± 0.013	0.046±0.009	0.026±0.005	0.015±0.001	0.033 ± 0.001	0.039 ± 0.007	7.2	3.8	2.6	1.5	1.2	4.4	2.7	2.4	1.9	5.8	4-61	λ	1-36
132	0.020 ± 0.003	0.048 ± 0.005	0.043±0.013	0.038±0.011	0.022±0.022	0.048 ± 0.000	0.051 ± 0.013	2.4	1.6	1.9	1.1	1.1	2.7	3.6	3.2	0.31	7.3	4-34	λ	7-46
150	0.011 ± 0.004	0.008 ± 0.002	0.007±0.002	0.007±0.002	0.005±0.001	0.012 ± 0.000	0.020 ± 0.001	0.7	0.5	0.6	0.5	1.7	0.57	1.6	1.1	0.70	0.77	3-53	K	1-9
158	0.016 ± 0.005	0.009 ± 0.001	0.021±0.004	0.011±0.002	0.013±0.001	0.031 ± 0.004	0.026 ± 0.002	0.6	1.1	0.7	0.8	0.8	1.4	1.3	0.75	1.4	2.4	3-53	K	1-9
159	>10	>10	>10	0.038±0.003	>10	0.011 ± 0.000	>10	N/A	N/A	<0.004	N/A	>928.4	N/A	N/A	N/A	N/A	N/A	3-30	K	3-20
165	0.009 ± 0.000	0.005 ± 0.001	0.009±0.001	0.013±0.002	0.002±0.001	0.034 ± 0.004	0.027 ± 0.006	0.6	1.0	1.4	0.2	0.8	0.34	0.71	0.51	0.54	1.7	1-58	K	3-20
170	0.024 ± 0.017	>10	0.493±0.047	0.012±0.003	0.550±0.204	0.025 ± 0.004	0.841 ± 0.103	>416.7	22.5	0.5	22.9	33.8	1.0	1.8	1.2	3987	2.6	5-51	K	2D-29
175	0.012 ± 0.001	0.007 ± 0.001	0.005±0.001	0.004±0.001	0.005±0.001	0.026 ± 0.000	0.017 ± 0.003	0.6	0.4	0.3	0.4	0.7	0.33	0.99	0.55	1.7	0.50	3-53	K	1-33 or 1D-33
222	0.010 ± 0.000	0.011 ± 0.001	0.015±0.003	0.007±0.001	0.007±0.000	0.019 ± 0.000	0.018 ± 0.001	1.1	1.2	0.7	0.7	0.9	0.25	1.5	0.20	1.4	0.52	3-53	K	3-20
253	0.012 ± 0.002	0.006 ± 0.002	0.003±0.001	0.006±0.002	0.003±0.001	0.055 ± 0.008	0.005 ± 0.001	0.5	0.3	0.5	0.3	0.1	0.51	1.6	0.78	1.9	0.96	1-58	K	3-20
269	0.004 ± 0.001	0.008 ± 0.001	0.009±0.003	0.012±0.004	0.0040.002	0.030 ± 0.000	0.021 ± 0.004	2.0	1.5	3.0	1.0	0.7	0.52	0.76	0.62	1.5	0.73	3-53	K	1-9
278	0.008 ± 0.004	>10	>10.00	0.005±0.001	4.527±0.747	0.014 ± 0.007	7.374 ± 1.397	>1250.0	>1250.0	0.6	565.9	539.2	1.6	6.3	1.5	22.0	6.4	1-18	K	1-39 or 1D-39
281	0.002 ± 0.000	>10	0.919±0.017	0.002±0.000	0.319±0.016	0.005 ± 0.001	1.494 ± 0.302	>5000.0	451.5	1.0	159.5	302.7	0.33	0.75	0.35	knocked out	0.65	3-7	K	2-24
316	0.003 ± 0.002	>10	0.003±0.001	0.004±0.001	0.004±0.002	0.018 ± 0.007	0.008 ± 0.001	>3333.3	1.3	1.3	0.7	0.4	0.38	1.0	0.69	1623	0.78	1-2	λ	2-8
318	0.018 ± 0.000	0.016 ± 0.007	0.020±0.006	0.008±0.003	0.016±0.011	0.029 ± 0.008	0.018 ± 0.003	0.9	0.8	0.4	1.5	0.6	3.5	11.4	2.8	2.0	5.6	1-58	K	3-20
384	0.002 ± 0.000	>10	0.070±0.015	0.001±0.000	0.009±0.001	0.004 ± 0.001	0.108 ± 0.035	>5000.0	27.5	0.5	4.5	25.8	0.65	0.98	0.84	knocked out	1.9	3-11	K	1-27
398	0.052 ± 0.024	>10	0.133±0.004	0.054±0.004	0.015±0.003	0.091 ± 0.004	0.237 ± 0.038	>192.3	2.5	1.0	0.3	2.6	1.1	7.3	5.5	1793	5.6	3-66	λ	2-8
AZD1061	0.007 ± 0.003	0.033 ± 0.020	N/A	0.004±0.001	N/A	0.013 ± 0.003	0.038 ± 0.006	5.1	N/A	0.6	N/A	2.9	3.9	6.7	3.8	6.7	6.9	N/A	N/A	N/A
AZD8895	0.003 ± 0.002	0.002 ± 0.011	N/A	0.001±0.000	N/A	0.005 ± 0.001	0.003 ± 0.000	0.7	N/A	0.3	N/A	0.5	1.00	2.1	3.7	3.9	1.5	N/A	N/A	N/A
AZD7442	0.002 ± 0.000	0.004 ± 0.002	N/A	0.002±0.000	N/A	0.009 ± 0.000	0.005 ± 0.000	2.0	N/A	1.0	N/A	0.6	2.0	13.0	6.3	2.2	2.4	N/A	N/A	N/A
REGN10987	0.014 ± 0.001	0.021 ± 0.011	N/A	0.008±0.000	N/A	0.032 ± 0.007	0.017 ± 0.009	1.5	N/A	0.6	N/A	0.5	0.38	0.36	0.35	0.13	0.38	N/A	N/A	N/A
REGN10933	0.002 ± 0.001	0.010 ± 0.007	N/A	0.001±0.000	N/A	0.004 ± 0.002	0.003 ± 0.001	5.0	N/A	0.5	N/A	0.6	0.81	2.2	1.8	0.44	0.74	N/A	N/A	N/A
ADG10	0.007 ± 0.004	0.009 ± 0.004	N/A	0.011±0.001	N/A	0.006 ± 0.000	0.026 ± 0.005	1.3	N/A	1.6	N/A	4.6	N/A	N/A	N/A	N/A	N/A	N/A	N/A	N/A
ADG20	0.002 ± 0.000	0.005 ± 0.001	N/A	0.003±0.001	N/A	0.004 ± 0.001	0.006 ± 0.001	2.5	N/A	1.5	N/A	1.4	N/A	N/A	N/A	N/A	N/A	N/A	N/A	N/A
ADG30	0.014 ± 0.000	0.048 ± 0.015	N/A	0.016±0.002	N/A	0.007 ± 0.002	0.033 ± 0.007	3.4	N/A	1.1	N/A	5.0	N/A	N/A	N/A	N/A	N/A	N/A	N/A	N/A
LY-CoV555	0.004 ± 0.001	>10	N/A	0.005±0.001	N/A	0.006 ± 0.002	8.311 ± 4.059	>2500.0	N/A	1.3	N/A	1284.3	N/A	N/A	N/A	N/A	N/A	N/A	N/A	N/A
LY-CoV16	0.026 ± 0.006	0.010 ± 0.001	N/A	0.006±0.001	N/A	0.034 ± 0.007	0.012 ± 0.002	0.4	N/A	0.2	N/A	0.4	N/A	N/A	N/A	N/A	N/A	N/A	N/A	N/A
S309	>10	0.238 ± 0.051	N/A	0.078±0.015	N/A	0.040 ± 0.005	0.113 ± 0.028	<0.024	N/A	<0.008	N/A	2.8	N/A	N/A	N/A	N/A	N/A	N/A	N/A	N/A

Table S2 Data collection and refinement statistics of RBD complexes. Related to X-ray data collection, structure determination and refinement, STAR Methods

[a] Values in parentheses are for highest-resolution shell.

Structure	RBD/222-278	L452R-RBD/75-253	T478K-RBD/45-253
PDB ID	7OR9	7ORB	7ORA
Data collection			
Space group	$P2_12_12_1$	$P2_1$	$P2_1$
Cell dimensions			
a, b, c (Å)	70.7, 114.5, 177.9	93.2, 149.4, 115.0	51.6, 182.4, 142.4
a, b, g (°)	90, 90, 90	90, 92.0, 90	90, 93.0, 90
Resolution (Å)	70–2.34 (2.38–2.34)[a]	75–2.50 (2.54–2.50)	61–2.60 (2.64–2.60)
R_{merge}	0.100 (---)	0.300 (---)	0.245 (---)
R_{pim}	0.030 (0.806)	0.058 (0.386)	0.101 (0.860)
I/s(I)	16.8 (0.8)	5.6 (0.4)	7.3 (0.6)
$CC_{1/2}$	0.999 (0.348)	0.993 (0.609)	0.986 (0.302)
Completeness (%)	86.2 (47.5)	99.8 (94.6)	90.5 (49.0)
Redundancy	11.6 (5.2)	28.1 (26.4)	6.7 (6.6)
Refinement			
Resolution (Å)	57–2.34	74–2.50	52–2.60
No. reflections	50501/2653	102853/5504	68969/3634
R_{work} / R_{free}	0.197/0.233	0.212/0.252	0.208/0.249
No. atoms			
Protein	8070	16156	16276
Ligand/ion/water	216	808	390
B factors (Å^2)			
Protein	61	64	66
Ligand/ion/water	67	73	57
r.m.s. deviations			
Bond lengths (Å)	0.002	0.003	0.002
Bond angles (°)	0.6	0.6	0.6

Table S3. NT50 titres against pseudo typed lentiviruses expressing full-length spike of SARS-CoV-2 strains Victoria and B.1.617.1, and live virus strains Victoria and B.1.617.2 (A) 34 convalescent plasma during early pandemic in UK (B) plasma from 18 patients infected with B.1.1.7 (C) serum from 14 patients infected with B.1.351 (D) serum from 17 patients infected with P.1 . The data underpinning the Victoria live virus neutralization curves of convalescent samples have been previously reported (Supasa et al, 2021). Related to Figure5 and 6.

		NT50 (Reciprocal plasma dilution)				NT50 ratio	
		Pseudo virus		Authentic virus			
		Victoria	B.1.617.1	Victoria	B.1.617.2	Victoria/B.1.617.1	Victoria/B.1.617.2
Early pandemic UK	Convalescent 1	99	<20	61	<20	>5.0	>3.1
	Convalescent 2	1098	165	689	41	6.7	16.6
	Convalescent 3	677	677	526	231	1.0	2.3
	Convalescent 4	992	817	409	445	1.2	0.9
	Convalescent 5	1016	54	369	136	18.8	2.7
	Convalescent 6	1417	820	1270	460	1.7	2.8
	Convalescent 7	716	115	274	124	6.2	2.2
	Convalescent 8	474	288	633	360	1.6	1.8
	Convalescent 9	N/A	N/A	667	81	N/A	8.2
	Convalescent 10	N/A	N/A	124	<20	N/A	>6.2
	Convalescent 11	N/A	N/A	102	127	N/A	0.8
	Convalescent 12	585	97	339	95	6.0	3.6
	Convalescent 13	362	214	331	55	1.7	6.0
	Convalescent 14	514	52	438	465	9.9	0.9
	Convalescent 15	8300	7086	6397	2916	1.2	2.2
	Convalescent 16	124	<20	44	<20	>6.2	>2.2
	Convalescent 17	1188	33	1115	239	35.6	4.7
	Convalescent 18	480	85	242	71	5.7	3.4
	Convalescent 19	78	19	29	<20	4.2	>1.5
	Convalescent 20	552	204	154	60	2.7	2.6
	Convalescent 21	894	135	487	76	6.6	6.4
	Convalescent 22	1596	497	438	236	3.2	1.9
	Convalescent 23	661	135	381	189	4.9	2.0
	Convalescent 24	2976	405	1647	900	7.4	1.8
	Convalescent 25	2609	750	913	747	3.5	1.2
	Convalescent 26	1677	424	1880	832	4.0	2.3
	Convalescent 27	1664	227	1464	829	7.3	1.8
	Convalescent 28	652	333	361	621	2.0	0.6
	Convalescent 29	3117	982	2859	1143	3.2	2.5
	Convalescent 30	1341	447	1109	425	3.0	2.6
	Convalescent 31	1518	454	811	556	3.3	1.5
	Convalescent 32	764	567	395	317	1.3	1.2
	Convalescent 33	N/A	N/A	1144	302	N/A	3.8
	Convalescent 34	1289	830	676	150	1.6	4.5
B.1.1.7	B.1.1.7 P3	101	27	143	39	3.7	3.7
	B.1.1.7-P4	22442	15436	88889	109481	1.5	0.8
	B.1.1.7 P5	1423	107	1839	384	13.3	4.8
	B.1.1.7 P6	655	69	562	54	9.5	10.4
	B.1.1.7 P7	2073	1623	2936	3049	1.3	1.0
	B.1.1.7 P8	2459	749	4696	535	3.3	8.8
	B.1.1.7 P9	2046	145	1777	533	14.1	3.3
	B.1.1.7 P10	3019	373	2484	1182	8.1	2.1
	B.1.1.7 P11	3243	205	1632	532	15.8	3.1
	B.1.1.7 P14	1444	665	1555	911	2.2	1.7
	B.1.1.7 P15	174	79	227	778	2.2	0.3
	B.1.1.7-P16	1463	292	2902	2016	5.0	1.4
	B.1.1.7-P17	803	415	3781	566	1.9	6.7
	B.1.1.7-P18	990	466	2641	732	2.1	3.6
	B.1.1.7-P19	575	54	775	211	10.7	3.7
	B.1.1.7-P20	1647	1197	2614	1509	1.4	1.7
	B.1.1.7-P22	422	172	390	182	2.4	2.1
	B.1.1.7-P23	2243	504	864	185	4.4	4.7
B.1.351	SA01	586	402	379	214	1.5	1.8
	SA02	564	876	597	629	0.6	0.9
	SA03	107	18	71	<20	5.9	>3.55
	SA04	824	1231	240	293	0.7	0.8
	SA05	166	27	67	<20	6.1	>3.35
	SA06	295	121	69	<20	2.4	>3.45
	SA07	1384	508	463	374	2.7	1.2
	SA08	360	239	641	30	1.5	21.7
	SA09	584	259	888	<20	2.3	>44.4
	SA10	57	98	80	<20	0.6	>4.4
	SA11	530	379	1234	83	1.4	14.9
	SA12	1026	1142	2148	390	0.9	5.5
	SA13	53	10	268	<20	5.1	>13.4
	SA14	678	511	595	123	1.3	4.8
P.1	P.1-1	274	125	86	<20	2.2	>4.3
	P.1-2	21	22	<20	<20	1.0	N/A
	P.1-3	108	58	20	<20	1.9	N/A
	P.1-4	152	116	29	<20	1.3	>1.4
	P.1-5	56	31	<20	<20	1.8	N/A
	P.1-6	1751	1039	2505	1311	1.7	1.9
	P.1-7	313	12	123	<20	25.1	>6.1
	P.1-8	151	100	40	<20	1.5	>2.0
	P.1-9	111	107	23	<20	1.0	>1.2
	P.1-10	107	19	<20	<20	5.5	N/A
	P.1-11	157	82	123	<20	1.9	>6.2
	P.1-12	62	48	<20	<20	1.3	N/A
	P.1-13	202	87	<20	<20	2.3	N/A
	P.1-14	121	39	87	<20	3.1	>4.3
	P.1-15	1555	2050	8199	2551	0.8	3.2
	P.1-16	337	194	828	333	1.7	2.5
	P.1-17	1489	364	1654	227	4.1	7.3

Table S4. NT50 titres against pseudo typed lentiviruses expressing full-length spike of SARS-CoV-2 strains Victoria and B.1.617.1, and strains Victoria and B.1.617.2 (A) Serum from 25 recipients of Pfizer-BioNTech vaccine. (B) Oxford-AstraZeneca vaccine. The data underpinning the Victoria live virus neutralization curves have been previously reported (Supasa et al, 2021). Related to Figure7.

	Day Post-boost	NT50 (Reciprocal plasma dilution)				NT50 ratio	
		Pseudovirus		Authentic virus			
		Victoria	B.1.617.1	Victoria	B.1.617.2	Victoria/B.1.671.1	Victoria/B.1.617.2
Pfizer1	7	1575	790	1149	540	2.0	2.1
Pfizer2	7	82	10	10	10	8.2	1.0
Pfizer3	7	1812	686	1727	644	2.6	2.7
Pfizer4	8	4675	3179	2234	3604	1.5	0.6
Pfizer5	7	3239	999	3016	992	3.2	3.0
Pfizer6	7	1994	1208	1521	875	1.7	1.7
Pfizer7	7	1466	973	609	636	1.5	1.0
Pfizer8	7	3115	953	4340	726	3.3	6.0
Pfizer9	7	888	405	1467	217	2.2	6.8
Pfizer10	7	2315	493	1757	338	4.7	5.2
Pfizer11	7	1418	307	860	138	4.6	6.2
Pfizer12	7	1643	619	1749	964	2.7	1.8
Pfizer13	7	2744	937	1851	932	2.9	2.0
Pfizer14	7	584	216	407	177	2.7	2.3
Pfizer15	8	1823	491	1285	466	3.7	2.8
Pfizer16	8	1094	216	1286	336	5.1	3.8
Pfizer17	8	2358	558	1810	811	4.2	2.2
Pfizer18	8	1872	1227	1198	474	1.5	2.5
Pfizer19	8	983	603	466	155	1.6	3.0
Pfizer20	8	1603	1156	1539	502	1.4	3.1
Pfizer21	9	347	34	184	39	10.3	4.7
Pfizer22	11	678	455	1061	586	1.5	1.8
Pfizer23	12	1149	297	1658	365	3.9	4.5
Pfizer24	12	1082	558	1155	1036	1.9	1.1
Pfizer25	15	3496	2494	8092	4256	1.4	1.9
AstraZeneca 1	28	489	333	495	235	1.5	2.1
AstraZeneca 2	28	440	345	580	308	1.3	1.9
AstraZeneca 3	28	90	12	253	10	7.2	25.3
AstraZeneca 4	28	349	311	183	101	1.1	1.8
AstraZeneca 5	28	681	56	432	121	12.2	3.6
AstraZeneca 6	28	169	30	764	134	5.6	5.7
AstraZeneca 7	28	228	127	133	10	1.8	13.3
AstraZeneca 8	28	333	81	257	57	4.1	4.5
AstraZeneca 9	28	134	106	501	194	1.3	2.6
AstraZeneca 10	28	93	133	357	217	0.7	1.6
AstraZeneca 11	14	192	116	334	90	1.7	3.7
AstraZeneca 12	14	88	51	250	54	1.7	4.6
AstraZeneca 13	14	373	218	122	26	1.7	4.8
AstraZeneca 14	14	188	91	212	41	2.1	5.1
AstraZeneca 15	14	572	87	789	69	6.6	11.5
AstraZeneca 16	14	202	156	538	201	1.3	2.7
AstraZeneca 17	14	763	208	1159	184	3.7	6.3
AstraZeneca 18	14	233	102	353	122	2.3	2.9
AstraZeneca 19	14	1031	443	975	224	2.3	4.3
AstraZeneca 20	14	188	64	169	30	2.9	5.7
AstraZeneca 21	14	224	49	155	29	4.5	5.4
AstraZeneca 22	14	367	49	152	39	7.6	3.9
AstraZeneca 23	14	96	43	126	27	2.3	4.7
AstraZeneca 24	14	612	102	293	223	6.0	1.3
AstraZeneca 25	14	67	32	94	10	2.1	9.4

Table S5. Primer sequences used to generate Pseudoviruses and RBD mutants. Related to Plasmid construction and pseudotyped lentiviral particles production, STAR METHODS.

Primer	Sequence (5′ to 3′)
Victoria insert fragments	
S247R_F	GCTGGCCCTGCACAGAAGATATCTTACACCAGGC
S247R_R	GCCTGGTGTAAGATATCTTCTGTGCAGGGCCAG
B.1.617.1 insert fragments	
E154K_F	CAACAAGAGCTGGATGAAGAGCGAGTTCCGCG
E154K_R	CGCGGAACTCGCTCTTCATCCAGCTCTTGTTG
L452R_F	GGAGGCAATTACAATTACCGGTACAGACTGTTCAGAAAG
L452R_R	CTTTCTGAACAGTCTGTACCGGTAATTGTAATTGCCTCC
E484Q_F	CCGTGTAATGGCGTGCAGGGCTTCAATTGCTAC
E484Q_R	GTAGCAATTGAAGCCCTGCACGCCATTACACGG
D614G_F	CGTGCTGTACCAGGGCGTGAATTGCACCG
D614G_R	CGGTGCAATTCACGCCCTGGTACAGCACG
P681R_F	CCCAGACCAATAGCCGTAGAAGAGCCAGAAG
P681R_R	CTTCTGGCTCTTCTACGGCTATTGGTCTGGG
E1072K/K1073R_F	CTACGTGCCTGCCCAGAAGAGGAATTTCACCACCGC
E1072K/K1073R_R	GCGGTGGTGAAATTCCTCTTCTGGGCAGGCACGTAG
T95I_F	GCGTGTACTTCGCCAGCATCGAGAAGAGCAATATC
T95I_R	GATATTGCTCTTCTCGATGCTGGCGAAGTACACGC
G142D_F	GTTCTGCAATGACCCTTTCCTGGATGTTTATTATCATAAGAACAAC
G142D_R	GTTGTTCTTATGATAATAAACATCCAGGAAAGGGTCATTGCAGAAC
Q1071H_F	CCTACGTGCCTGCCCATGAGAAGAATTTCACCA
Q1071H_R	TGGTGAAATTCTTCTCATGGGCAGGCACGTAGG
B.1.617.2 insert fragments	
T19R_F	GCAGCCAGTGCGTGAATCTGAGGACCAGAACCCAG
T19R_R	CTGGGTTCTGGTCCTCAGATTCACGCACTGGCTGC
Del156-158_F	CAAGAGCTGGATGGAGAGCGTATATTCGTCGGCTAATAATTGCCC
Del156-158_R	GGGCAATTATTAGCCGACGAATATACGCTCTCCATCCAGCTCTTG
D950N_F	CTGGGCAAGCTGCAGAACGTGGTGAATCAGAATG
D950N_R	CATTCTGATTCACCACGTTCTGCAGCTTGCCCAG
B.1.1.519 insert fragments	
T478K_F	TACCAGGCCGGCAGCAAACCGTGTAATGG
T478K_R	CCATTACACGGTTTGCTGCCGGCCTGGTA
T732A_F	GAAATATTACCAGTCTCCATGGCCAAGACCAGCGTGG
T732A_R	CCACGCTGGTCTTGGCCATGGAGACTGGTAATATTTC
B.1.429 insert fragments	
S13I_F	CTGCCTCTGGTGAGCATCCAGTGCGTGAATC
S13I_R	GATTCACGCACTGGATGCTCACCAGAGGCAG
W152C_F	CATAAGAACAACAAGAGCTGCATGGAGAGCGAGTTCC
W152C_R	GGAACTCGCTCTCCATGCAGCTCTTGTTGTTCTTATG
P681H_F	ACCCAGACCAATAGCCATAGAAGAGCCAGAAGC
P681H_R	GCTTCTGGCTCTTCTATGGCTATTGGTCTGGGT
pcDNA3.1 vector	
pcDNA3.1_BamHI_F	GGATCCATGTTCCTGCTGACCACCAAGAG
pcDNA3.1_Tag_S_EcoRI_R	GAATTCTCACTTCTCGAACTGAGGGTGGC
pcDNA3.1_Tag_S_EcoRI_F	GCCACCCTCAGTTCGAGAAGTGAGAATTC
pcDNA3.1_BamHI_R	CTCTTGGTGGTCAGCAGGAACATGGATCC
pNEO vector	
PV_RBD_F	TGATGGGTTGCGTAGCTGAAACCGGTCACCATCACCATCACCATACCAATCTGTGCCCTTTCGGCGAGGTGTTC
PV_RBD_R	CTGGAACAGCACCTCCAGGGTACCTCACTTTTTGCCGCACACGGTAGCGGGAGC
pNEO_F	GCTGGTTGTTGTGCTGTCTCATC
pNEO_R	CGTAAAAGGAGCAACATAG